Master's Thesis

Màster Universitari en Enginyeria Industrial

Development of estimated Grid Frequency in Disturbed Converter-Based Power systems by PLL State Variable Feedback

April 2021

Author: Ignacio Glenny Crende

Supervisor UPC: Oriol Gomis Bellmunt

Supervisor HTW: Horst Schulte

ETSEIB

Escola Tècnica Superior
d'Enginyeria Industrial de Barcelona

htw.

Hochschule für Technik
und Wirtschaft Berlin

University of Applied Sciences

Abstract

English

The first part considers a model-based extension of least mean square phase-locked loop (LMS PLL) control design with a Takagi-Sugeno Static Prefilter in simulation environment including an I-augmentation (Goldschmidt, Schulte, "Estimation of Grid Frequency in Disturbed Converter-Based Power Systems by PLL State Variable Feedback", IFAC 2020) and Standard Static Prefilter (Föllinger 2013 "Regelungstechnik", 11th Edition).

The second part focuses on result comparison and analysis of the three different implemented PLLs. The response of the different PLLs is analyzed under frequency variation conditions and during phase-to-phase shortcircuits, both with a low and high presence of 5th and 7th harmonics. The tool used for modelling and simulating is MatLab® 2019a.

The Takagi-Sugeno Static Prefilter presents certain advantages compared to the I-Augmented PLL and the Standard Static Prefilter PLL, showing faster settling times during fault that the former and less steady state error than the latter. Ways for improving the results of the Takagi-Sugeno Static Prefilter are presented.

Castellano

La primera parte de este Trabajo de Fin de Máster contempla una extensión de una LMS PLL (bucle seguidor de fase por mínimos cuadrados) con un prefiltro estático Takagi-Sugeno. El ambiente de simulación incluye también una PLL ampliada con un integrador (Goldschmidt, Schulte, "Estimation of Grid Frequency in Disturbed Converter-Based Power Systems by PLL State Variable Feedback", IFAC 2020) y otra ampliada con un prefiltro estático estándar (Föllinger 2013 "Regelungstechnik", 11th Edition).

La segunda parte de este trabajo se centra en la comparación y análisis de los resultados obtenidos por cada una de las tres PLL implementadas. Se analiza la respuesta de las distintas PLL ante eventos de variación de frecuencia y cortocircuitos fase-fase con baja y alta presencia de los harmónicos quinto y séptimo. La herramienta usada para llevar a cabo la modelización y simulación de los distintos sistemas involucrados es MatLab® 2019a.

El prefiltro estático Takagi-Sugeno muestra ciertas ventajas respecto a las otras PLL, mostrando tiempos de estabilización menores que la aumentada con integrador y errores en estado estacionario menores que el prefiltro estático estándar. Se presentan también posibles mejoras que podrían aplicarse al prefiltro estático Takagi-Sugeno para obtener mejores resutlados.

Contents

List of Tables

List of Figures

Chapter 1

Introduction

1.1 Renewable Energy Sources

Renewable energy sources like Solar Photo-Voltaic or Wind Turbines present an intermittence that adds unreliability to the electrical grid. These energy availability issues can be solved via higher interconnectivity between grids and energy storage systems, but these solutions increase the cost and the presence of power electronics in the grid [3].

Even without resorting to energy storage systems, renewable energy sources require power electronics components in order to transfer their power to the grid. This increase in power electronics components carries with itself new challenges for the grid; issues like harmonic injection or the lack of physical inertia become more relevant as the share of renewable energy sources in the grid increases [4, 5].

Consequently, when thinking about the integration of renewable energy sources in the grid one must not consider that the current conditions will remain in place. Robust system control is needed in order to guarantee that the grid is able to function even during unfavourable conditions.

1.2 Control methods for renewable energy integration

Increasing renewable energy integration in the grid and the industrial development that follows threatens the stability of the electrical system [6]. With their share increasing so does their importance and the need for them to become active control units regarding grid forming and stabilization [2].

One must be able to reconstruct the main harmonic and inject power in phase even under unfavourable conditions. Different methods for doing this are through compression sampling on the original harmonic and interharmonics signals respectively as seen in [6], through a cubic spline interpolation algorithm [7] or through a least mean squares filter as seen in [2]. This last approach will be the one used in this thesis.

The increase in renewable energy integration and in the use of microgrids translates into higher fault risks and uncertainties [8], meaning that designing fault-tolerant control systems becomes necessary.

Robust control is an approach in controller design that explicitly deals with uncertainty in a system. Given the aforementioned conditions that are to be expected in microgrids and in smaller grids when renewable energy source's share in the power mix increases, resorting to robust control design in order to deal with the uncertainties caused by it becomes a necessity [8].

1.3 Introduction to PLLs

Phase Locked Loop (PLL) algorithms are a proven method to estimate current first harmonic phase angle and fequency of an electrical grid. The most widely used method for ensuring nearly ideal conditions in grids, avoiding distortion or unbalance, is the synchronous reference frame PLL in combination with a classic proportional integral (PI) controller [2, 9, 10].

However, a second harmonic of the voltage vector can be caused by the negative sequence components when under unbalanced grid conditions. When aiming for a robust operation, feedback dynamics must be limited significantly, resulting in a low response speed. In recent years, modified PLLs based on pre-processing methods that remove unbalanced components and high-order harmonics [2]. Two pre-processing methods can be distinguished:

1. *Type 1 pre-processing methods* first use the disturbed signal to form symmetrical components and decouple particular harmonics afterwards.
2. *Type 2 pre-processing methods* filter out the desired harmonics initially and then form the symmetrical components.

The issue with Type 1 PLLs like the decoupled double synchronous reference frame PLL (dd-SRF-PLL) proposed in [11] or the multi synchronous reference frame PLL (md-SRF-PLL) in [12] is that only a few components can be decoupled, while the effort increases proportionally. In Type 2 methods the desired signal is filtered out at the beginning, as seen in [13, 14] where it is done via a least mean square (LMS) filter.

The approach used in this Thesis is the one seen in [2], which is part of the Type 2 method. However, the final frequency reconstruction is done via a novel state feedback controller scheme based on linear matrix inequality (LMI).

1.4 Objectives and scope

The main objective of the thesis is to develop a Takagi-Sugeno Static Prefilter PLL and implement it in a MatLab ® 2019a Simulink environment in order to compare its performance with other PLLs.

The simulation and analysis process has been divided four different parts:

1. *Development of the Takagi-Sugeno Static Prefilter PLL*, done with MatLab® 2019a Simulink and the SimPowerSystems Toolbox.
2. *The implementation of the Takagi-Sugeno Static Prefilter PLL in a simulation environment with a LMS filter and two other PLLs*, done with MatLab® 2019a Simulink and the SimPowerSystems Toolbox.
3. *Comparison of the PLLs response to different conditions regarding grid events like strong harmonics injection, shortcircuits and frequency variation events*, done with MatLab® 2019a Simulink and the SimPowerSystems Toolbox.
4. *Analysis of the simulation results.*

Chapter 2

Theoretical Base

2.1 State Space model and control

In a state space model, a system is defined as seen in equations 2.1-2.2 that follow.

$$\dot{\mathbf{x}} = \mathbf{f}(\mathbf{x}, \mathbf{u}, \mathbf{u_d}) = \mathbf{Ax} + \mathbf{Bu} + \mathbf{Eu_d} \tag{2.1}$$
$$\mathbf{y} = \mathbf{g}(\mathbf{x}, \mathbf{u}, \mathbf{u_d}) = \mathbf{Cx} + \mathbf{Du} + \mathbf{Fu_d} \tag{2.2}$$

Where

- $\mathbf{x}$ is the state vector, holding the value of each state variable
- $\mathbf{u}$ is the input vector, that allows state variation by controlling and altering the system
- $\dot{\mathbf{x}} = \mathbf{f}(\mathbf{x_c}, \mathbf{u_c}, \mathbf{u_{d,c}})$ is the state derivatives vector
- $\mathbf{y}$ is the system output vector, which is defined based on the variables we wish to observe

The matrices that represent the state space model are built out of a set of differential equations.

2.2 Linearization

Three steps are necessary for the linearization of a non-linear model around an equilibrium point.

First, a stationary working point must be defined:

$$\dot{\mathbf{x}} = \mathbf{f}(\mathbf{x_c}, \mathbf{u_c}, \mathbf{u_{d,c}}) = \mathbf{0} \tag{2.3}$$
$$\mathbf{y} = \mathbf{g}(\mathbf{x_c}, \mathbf{u_c}, \mathbf{u_{d,c}}) \tag{2.4}$$

The objective is for the overall system to reach a state of equilibrium after a time $t \to \infty$. As seen in 2.5, given a constant input u_c and $u_{d,c}$ the state derivatives $\dot{x}$ tend towards 0 and the state variables x reach a constant value x_c.

$$\mathbf{0} = \mathbf{A}\mathbf{x_c} + \mathbf{B}\mathbf{u_c} + \mathbf{E}\mathbf{u_{d,c}} \tag{2.5}$$
$$\mathbf{y} = \mathbf{C}\mathbf{x_c} + \mathbf{D}\mathbf{u_c} + \mathbf{F}\mathbf{u_{d,c}} \tag{2.6}$$

Second, input, status and output variables shall be replaced by the difference variables $\mathbf{\Delta u}$, $\mathbf{\Delta x}$ and $\mathbf{\Delta u_d}$ due to the linearized state space model being valid only in a sufficiently narrow environment around the equilibrium point.

$$\mathbf{\Delta u} = \mathbf{u} - \mathbf{u_c} \tag{2.7}$$
$$\mathbf{\Delta x} = \mathbf{x} - \mathbf{x_c} \tag{2.8}$$
$$\mathbf{\Delta u_d} = \mathbf{u_d} - \mathbf{u_{d,c}} \tag{2.9}$$

Third, a vector differential equation is developed following Taylor's theorem in the immediate area around the stationary working point $(\mathbf{u_c}, \mathbf{x_c}, \mathbf{u_{d,c}})$, following the general approach in matrix form shown below:

$$\begin{aligned}\mathbf{\Delta \dot{x}} = \mathbf{f}(\mathbf{x_c}, \mathbf{u_c}, \mathbf{u_{dc}}) + \left.\frac{\partial \mathbf{f}(\mathbf{x}, \mathbf{u}, \mathbf{u_d})}{\partial \mathbf{x}}\right|_{\mathbf{x_c}, \mathbf{u_c}, \mathbf{u_{d,c}}} \mathbf{\Delta x} + \left.\frac{\partial \mathbf{f}(\mathbf{x}, \mathbf{u}, \mathbf{u_d})}{\partial \mathbf{u}}\right|_{\mathbf{x_c}, \mathbf{u_c}, \mathbf{u_{d,c}}} \mathbf{\Delta u} \\ + \left.\frac{\partial \mathbf{f}(\mathbf{x}, \mathbf{u}, \mathbf{u_d})}{\partial \mathbf{u_d}}\right|_{\mathbf{x_c}, \mathbf{u_c}, \mathbf{u_{d,c}}} \mathbf{\Delta u_d} + \mathbf{r_x}(\mathbf{\Delta x}, \mathbf{\Delta u}, \mathbf{\Delta u_d})\end{aligned} \tag{2.10}$$

$$\begin{aligned}\mathbf{\Delta y} = \mathbf{g}(\mathbf{x_c}, \mathbf{u_c}, \mathbf{u_{dc}}) + \left.\frac{\partial \mathbf{g}(\mathbf{x}, \mathbf{u}, \mathbf{u_d})}{\partial \mathbf{x}}\right|_{\mathbf{x_c}, \mathbf{u_c}, \mathbf{u_{d,c}}} \mathbf{\Delta x} + \left.\frac{\partial \mathbf{g}(\mathbf{x}, \mathbf{u}, \mathbf{u_d})}{\partial \mathbf{u}}\right|_{\mathbf{x_c}, \mathbf{u_c}, \mathbf{u_{d,c}}} \mathbf{\Delta u} \\ + \left.\frac{\partial \mathbf{g}(\mathbf{x}, \mathbf{u}, \mathbf{u_d})}{\partial \mathbf{u_d}}\right|_{\mathbf{x_c}, \mathbf{u_c}, \mathbf{u_{d,c}}} \mathbf{\Delta u_d} + \mathbf{r_y}(\mathbf{\Delta x}, \mathbf{\Delta u}, \mathbf{\Delta u_d})\end{aligned} \tag{2.11}$$

Vectors $\mathbf{r_x}(\mathbf{\Delta x}, \mathbf{\Delta u}, \mathbf{\Delta u_d})$ and $\mathbf{r_y}(\mathbf{\Delta x}, \mathbf{\Delta u}, \mathbf{\Delta u_d})$ represent second and higher order terms. These can be neglected compared to the terms of the first order if the difference variables $\mathbf{\Delta x}$, $\mathbf{\Delta u}$ and $\mathbf{\Delta u_d}$ are sufficiently small in terms of amount.

If the series expansion is separated according to the function matrices of the state space model, said function matrices can be derived individually as seen below in equations (2.12-2.15). For the purpose of this Thesis, matrices $\mathbf{E}$ and $\mathbf{F}$ are considered null, and in order to avoid including unnecessary information the calculation of $\mathbf{E_c}$ and $\mathbf{F_c}$ are not shown.

$$\left.\frac{\partial \mathbf{f}(\mathbf{x},\mathbf{u},\mathbf{u_d})}{\partial \mathbf{x}}\right|_{\mathbf{x_c},\mathbf{u_c},\mathbf{u_{d,c}}} = \mathbf{A_c} = \begin{pmatrix} \frac{\partial f_1(x_c,u_c,u_{d,c})}{\partial x_1} & \dots & \frac{\partial f_1(x_c,u_c,u_{d,c})}{\partial x_n} \\ \vdots & \ddots & \vdots \\ \frac{\partial f_n(x_c,u_c,u_{d,c})}{\partial x_1} & \dots & \frac{\partial f_n(x_c,u_c,u_{d,c})}{\partial x_n} \end{pmatrix} \tag{2.12}$$

$$\left.\frac{\partial \mathbf{f}(\mathbf{x},\mathbf{u},\mathbf{u_d})}{\partial \mathbf{u}}\right|_{\mathbf{x_c},\mathbf{u_c},\mathbf{u_{d,c}}} = \mathbf{B_c} = \begin{pmatrix} \frac{\partial f_1(x_c,u_c,u_{d,c})}{\partial u_1} & \dots & \frac{\partial f_1(x_c,u_c,u_{d,c})}{\partial u_m} \\ \vdots & \ddots & \vdots \\ \frac{\partial f_n(x_c,u_c,u_{d,c})}{\partial u_1} & \dots & \frac{\partial f_n(x_c,u_c,u_{d,c})}{\partial u_m} \end{pmatrix} \tag{2.13}$$

$$\left.\frac{\partial \mathbf{g}(\mathbf{x},\mathbf{u},\mathbf{u_d})}{\partial \mathbf{x}}\right|_{\mathbf{x_c},\mathbf{u_c},\mathbf{u_{d,c}}} = \mathbf{C_c} = \begin{pmatrix} \frac{\partial g_1(x_c,u_c,u_{d,c})}{\partial x_1} & \dots & \frac{\partial g_1(x_c,u_c,u_{d,c})}{\partial x_n} \\ \vdots & \ddots & \vdots \\ \frac{\partial g_n(x_c,u_c,u_{d,c})}{\partial x_1} & \dots & \frac{\partial g_n(x_c,u_c,u_{d,c})}{\partial x_n} \end{pmatrix} \tag{2.14}$$

$$\left.\frac{\partial \mathbf{g}(\mathbf{x},\mathbf{u},\mathbf{u_d})}{\partial \mathbf{u}}\right|_{\mathbf{x_c},\mathbf{u_c},\mathbf{u_{d,c}}} = \mathbf{D_c} = \begin{pmatrix} \frac{\partial g_1(x_c,u_c,u_{d,c})}{\partial u_1} & \dots & \frac{\partial g_1(x_c,u_c,u_{d,c})}{\partial u_m} \\ \vdots & \ddots & \vdots \\ \frac{\partial g_n(x_c,u_c,u_{d,c})}{\partial u_1} & \dots & \frac{\partial g_n(x_c,u_c,u_{d,c})}{\partial u_m} \end{pmatrix} \tag{2.15}$$

$$\Delta\dot{x} = A_c\Delta x + B_c\Delta u \tag{2.16}$$

$$\Delta y = C_c\Delta x + D_c\Delta u \tag{2.17}$$

With

$$\Delta u = u - u_c \tag{2.18}$$

$$\Delta x = x - x_c \tag{2.19}$$

A graphic representation of the linearised state space model can be seen in figure 2.1 that follows.

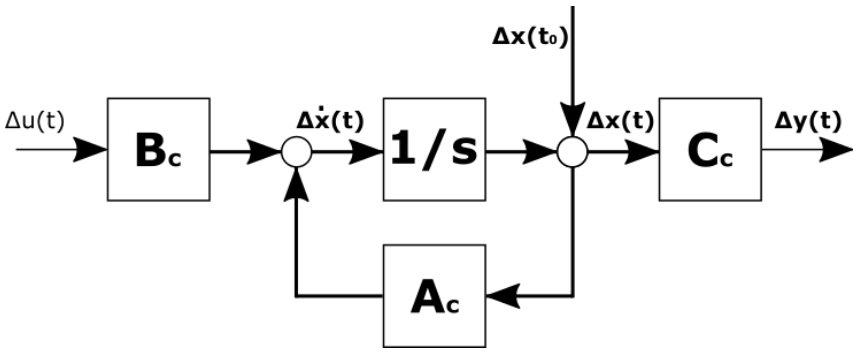

Figure 2.1: Block diagram of the linearised state space model.

2.3 Invertibility and Moore-Pensore inverse

An arbitrary square *n-by-n* matrix $\mathbf{A}$ can be considered invertible if a square *n-by-n* matrix $\mathbf{B} = \mathbf{A^{-1}}$ exists in a way that equation 2.20 holds true.

$$\mathbf{A\ B = B\ A = I_n} \tag{2.20}$$

Where $\mathbf{I_n}$ is an *n-by-n* square identity matrix.

This invertibility theorem imposes several equivalent statements. That is, if a matrix is invertible, these conditions are also true. Some of them are, for example, having a non-zero determinant, having non-zero eigenvalues or having linearly independent columns, among others.

These conditions can be very restrictive. Not all state space representations of systems are invertible.

For matrices that don't fulfil full invertibility requirements, a generalized inverse (or pseudo-inverse or Moore-Penrose inverse) can be defined.

For an *m-by-n* arbitrary matrix $\mathbf{A}$, its pseudo-inverse $\mathbf{A}^+$ is an *n-by-m* matrix that satisfies the Moore-Penrose conditions as seen in equations 2.21-2.24.

$$\mathbf{A\ A^+\ A = A} \tag{2.21}$$
$$\mathbf{A^+\ A\ A^+ = A^+} \tag{2.22}$$
$$\mathbf{(RQ)^* = RQ} \tag{2.23}$$
$$\mathbf{(QR)^* = QR} \tag{2.24}$$

When a matrix $\mathbf{A}$ is invertible, its Moore-Penrose inverse will equal its inverse so that $\mathbf{A^+ = A^{-1}}$. Unlike inverse matrices $\mathbf{A^{-1}}$ of invertible matrices $\mathbf{A}$, pseudo-inverses cannot always be calculated using an algebraic formula. In this Master's thesis pseudo-inverses will be calculated using Matlab 2019a's *pinv(argument)* function, based on Singular Value Decomposition.

2.4 Per Unit (p.u.) system

The Per Unit (p.u.) system is used for simplifying calculations and readings related to electrical power systems. The main advantages of the p.u. system are as follows:

- *Values of the same variable (voltage, current...) are similar.* This simplifies the comparison of systems that differ in size.
- *Calculations are simpler.* Some systems require you to take into account different voltage levels (i.e. working with a transformer). By using different p.u. base values, bringing the different voltage values to a similar scale, the calculations are simplified significantly.

- *Three-phase calculations are simplified.* Some expressions used in most three-phase calculations disappear when working in p.u., simplifying both calculations and expressions.

The corresponding values in p.u. are obtained by dividing the actual value in the standard *abc* reference by a predefined base value. The different base values S_B, V_B, I_B and Z_B (for apparent power, tension, current and impedance) are related via the following equations:

$$S_B = \sqrt{3} V_B I_B \tag{2.25}$$

$$V_B = \sqrt{3} Z_B I_B \tag{2.26}$$

$$I_B = \frac{S_B}{\sqrt{3} V_B} \tag{2.27}$$

$$Z_B = \frac{V_B}{\sqrt{3} I_B} = \frac{V_B^2}{S_B} \tag{2.28}$$

Once the base values are defined, calculating the p.u. equivalent s, v, i and z of the standard values S, V, I and Z is done by calculating the quotient of the standard value divided by the base value.

$$s = \frac{S}{S_B} \tag{2.29}$$

$$v = \frac{V}{V_B} \tag{2.30}$$

$$i = \frac{I}{I_B} \tag{2.31}$$

$$z = \frac{Z}{Z_B} \tag{2.32}$$

2.5 Phase Locked Loop

2.5.1 General information about PLLs

Phase Locked Loop (PLL) algorithms are a proven method to estimate the current first harmonic phase angle and frequency of the electrical grid [2]. Accurate phase information of the utility voltages allows a better control of the power factor [9].

2.5.2 Regulator calculation

The regulator is defined so that it stabilizes the state control, keeping the eigenvalues of the closed loop system to the left of the j-axis [15].

This is done following a pole placement methodology as explained in [1]. Pole placement objectives are formulated via a LMI-based characterization and an extended Lyapunov theorem applied to the resulting regions.

A working region based on the set $S(\alpha, r, \theta)$ of complex numbers $x+jy$ must be defined, and the poles for the system are found through an LMI optimization problem such that the conditions seen in 2.33 are met [1].

$$\begin{aligned} &x < -\alpha < 0 \\ &+jy| < r \\ &tan\theta x < -|y| \end{aligned} \tag{2.33}$$

This region is represented in figure 2.2 below.

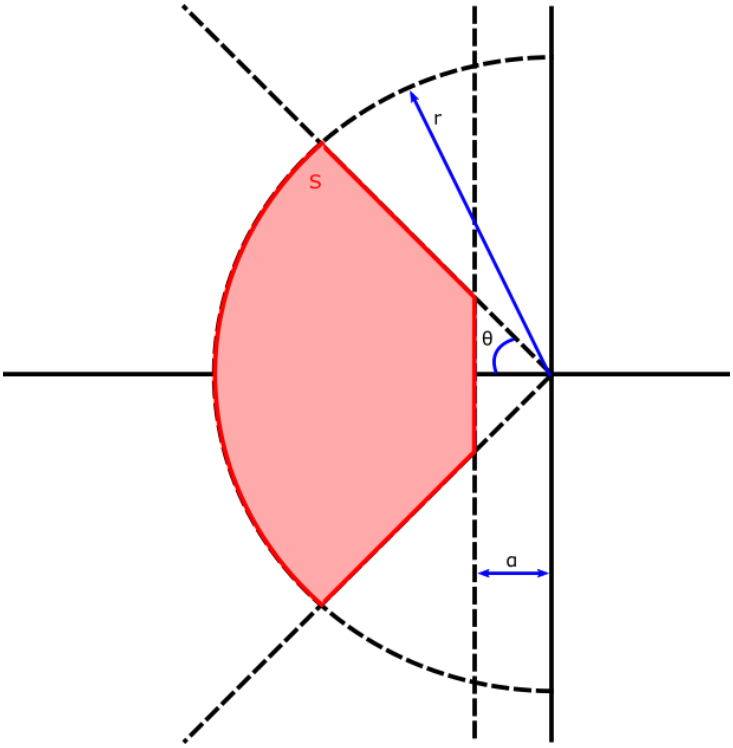

Figure 2.2: Region $S(\alpha, r, \theta)$ as seen in [1]

In this thesis, poles are defined working with a set $S(\alpha, \beta, \theta)$ of complex numbers $x + jy$ such that the conditions seen in 2.34 limit pole placement region. Figure 2.3 shows a graphical representations of these conditions in the complex plane.

$$\begin{aligned} &x < -\alpha < 0 \\ &-\alpha > \ x \ > -\beta \\ &tan\theta x < -|y| \end{aligned} \tag{2.34}$$

For the I-augmented PLL, the method differs slightly. According to eq. 2.47, the regulator is obtained in the form seen in eq. 2.35, where $\hat{\mathbf{R}}$ and $\mathbf{R_I}$ are given numerically.

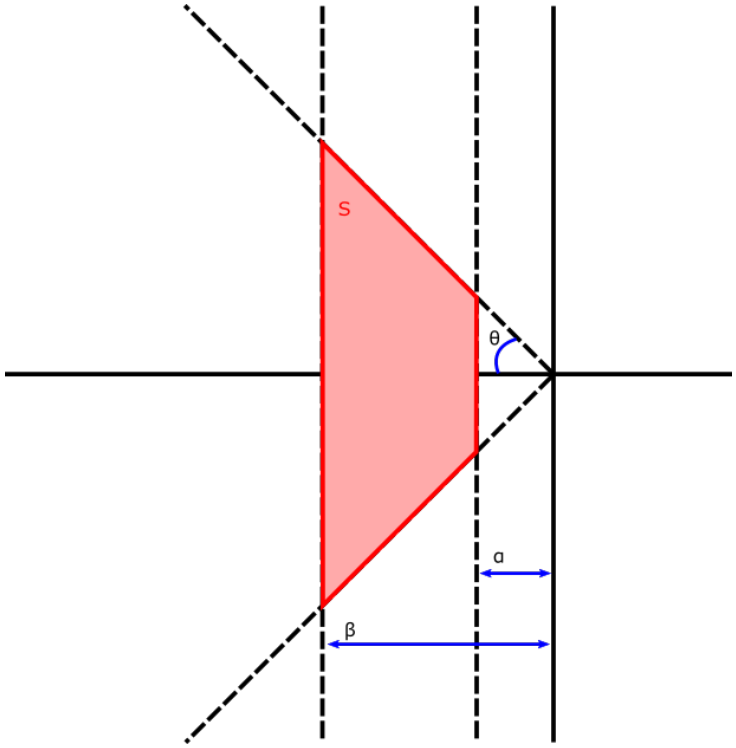

Figure 2.3: Region $S(\alpha, \beta, \theta)$ as seen in [2].

$$\mathbf{R} = \begin{bmatrix} \hat{\mathbf{R}} & -\mathbf{R_I} \end{bmatrix} \tag{2.35}$$

$$\hat{\mathbf{R}} = \mathbf{R_X} + \mathbf{R_P}\mathbf{C_R} \tag{2.36}$$

In order to determine the still unknown matrices $\mathbf{R_X}$ and $\mathbf{R_P}$, the normal case $p = q$ where the number of controlled variables is equal to the number of control variables is assumed.

2.5.3 I-augmented PLL

In this proposal seen in [2], in addition to the state feedback, one feeds back the output vector $\mathbf{y}_R$ of controlled variables (assumed measurable). This is then compared with the command vector $\mathbf{w}$, obtaining a control difference vector $\dot{\mathbf{e}}$. As seen in figure 2.4, the difference vector $\dot{\mathbf{e}}$ is then put through a PI controller. In order to avoid complicating the picture unnecessarily, the drawing of an observer for the state vector $\mathbf{x}$ was omitted. If necessary, in order to estimate $\mathbf{x}$ it should be inserted into the inner loop .

The PI state controller is given by the equation 2.37 below [15].

$$\mathbf{u}_S = \mathbf{R}_P\dot{\mathbf{e}} + \mathbf{R}_I\mathbf{e} \tag{2.37}$$

Where the control difference vector is

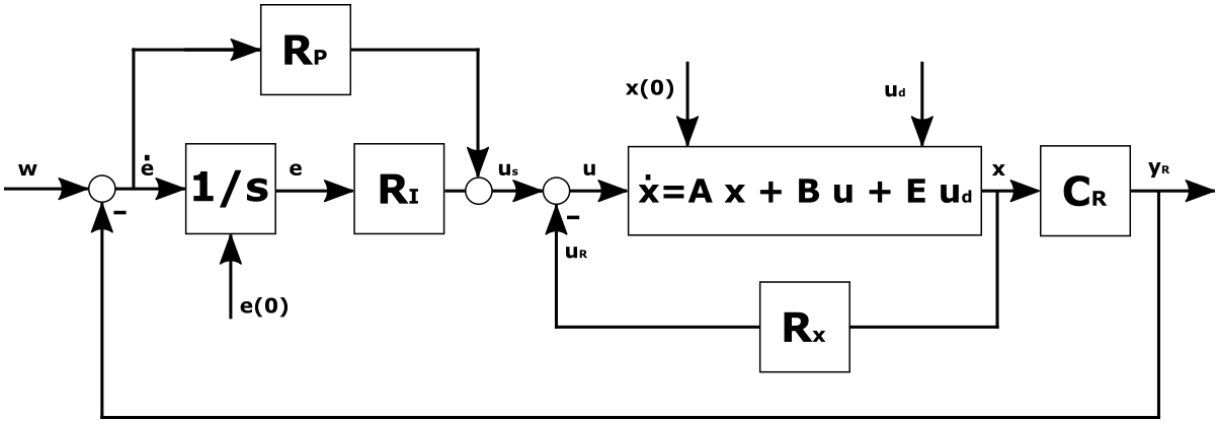

Figure 2.4: State control with additional PI controller.

$$\dot{\mathbf{e}} = \mathbf{w} - \mathbf{y}_R \tag{2.38}$$

It is integrated, so that the PI state controller contains q integrating elements, where q is the number of controlled variables. The designation is somewhat different from that of the classical control loop, because this is useful for the mathematical description of the overall system.

The purpose of this arrangement is that if the entire system is stabilised by the controllers $\mathbf{R}_x$, $\mathbf{R}_p$ and $\mathbf{R}_I$ the control difference vector $\dot{\mathbf{e}} = 0$ in the steady state. This in turn translates to $\mathbf{y}_R = \mathbf{w}$. This allows to eliminate the influence of the disturbance vector in the steady state and make the control vector $\mathbf{w}$ equal to the guidance vector $\mathbf{y}_R$ [15].

The regulation equations are as follows:

$$\dot{\mathbf{x}} = \mathbf{A}\mathbf{x} + \mathbf{B}\mathbf{u} + \mathbf{E}\mathbf{z} \tag{2.39}$$
$$\mathbf{y_R} = \mathbf{C_R}\mathbf{x} \tag{2.40}$$
$$\dot{\mathbf{e}} = -\mathbf{C_R}\mathbf{x} \tag{2.41}$$
$$\mathbf{u} = -\mathbf{R_X}\mathbf{x} - \mathbf{R_P}\mathbf{C_R}\mathbf{x} + \mathbf{R_I}\mathbf{e} \tag{2.42}$$

The effect of external variables regarding stabilisation is not relevant, so they will be set to zero, meaning that the regulation equations end up as follows:

$$\mathbf{w} = 0$$
$$\mathbf{z} = 0$$

$$\dot{\mathbf{x}} = \mathbf{A}\mathbf{x} + \mathbf{B}\mathbf{u} \tag{2.43}$$
$$\dot{\mathbf{e}} = -\mathbf{C_R}\mathbf{x} \tag{2.44}$$
$$\mathbf{u} = -\mathbf{R_X}\mathbf{x} - \mathbf{R_P}\mathbf{C_R}\mathbf{x} + \mathbf{R_I}\mathbf{e} \tag{2.45}$$

Which can be written as

$$\begin{bmatrix}\dot{\mathbf{x}}\\ \dot{\mathbf{e}}\end{bmatrix} = \begin{bmatrix}\mathbf{A} & \mathbf{0}\\ -\mathbf{C_R} & \mathbf{0}\end{bmatrix} \cdot \begin{bmatrix}\mathbf{x}\\ \mathbf{e}\end{bmatrix} + \begin{bmatrix}\mathbf{B}\\ \mathbf{0}\end{bmatrix} \mathbf{u} \tag{2.46}$$

$$\mathbf{u} = -\begin{bmatrix}\mathbf{R_X} + \mathbf{R_P C_R} & -\mathbf{R_I}\end{bmatrix} \cdot \begin{bmatrix}\mathbf{x}\\ \mathbf{e}\end{bmatrix} \tag{2.47}$$

The extended controller matrix in eq. 2.47 is of the type $(p, n+q)$, while the extended distance matrix of eq. 2.46 is of the type $(n+q, n+q)$. In order to guarantee that the extended controller can be designed by pole positioning or as a Riccati controller the extended system's controllability must be proved [2].

For the extended distance as seen in eq. 2.46 to be controllable it is necessary that the original model $(\mathbf{A}, \mathbf{B})$ is controllable and that equation 2.48 holds.

$$range \begin{bmatrix}\mathbf{A} & \mathbf{B}\\ -\mathbf{C_R} & \mathbf{0}\end{bmatrix} = n + q \tag{2.48}$$

This can be proved by means of Hautus' controllability criteria [15]. According to this, the extended distance is controllable exactly when

$$\rho = range \begin{bmatrix}\lambda_\mathbf{i}\mathbf{I_n} - \mathbf{A} & \mathbf{0} & \mathbf{B}\\ \mathbf{C_R} & \lambda_\mathbf{i}\mathbf{I_q} & \mathbf{0}\end{bmatrix}$$

has the maximum value $n+q$, namely for the eigenvalues $\lambda_1, ..., \lambda_n$ of the original path and the q-fold eigenvalue $\lambda_0 = 0$ newly added by the I-members. Since column swaps do not change the rank, one can also write ρ as seen in equation 2.49 below.

$$\rho = range \begin{bmatrix}\lambda_\mathbf{i}\mathbf{I_n} - \mathbf{A} & \mathbf{B} & \mathbf{0}\\ \mathbf{C_R} & \mathbf{0} & \lambda_\mathbf{i}\mathbf{I_q}\end{bmatrix} \tag{2.49}$$

If one sets $\lambda_i = 0$ where it is the same whether it is an eigenvalue of the original model or λ_0 then

$$\begin{aligned}\rho &= range \begin{bmatrix}-\mathbf{A} & \mathbf{B} & \mathbf{0}\\ \mathbf{C_R} & \mathbf{0} & \mathbf{0}\end{bmatrix}\\ &= range \begin{bmatrix}-\mathbf{A} & \mathbf{B}\\ \mathbf{C_R} & \mathbf{0}\end{bmatrix}\end{aligned}$$

The deletion of zero columns does not change the rank of a given matrix. Multiplication by a regular matrix also leaves the rank unchanged, and as such ρ can be presented as seen in equation 2.50 below.

$$\begin{bmatrix} -\mathbf{A} & \mathbf{B} \\ \mathbf{C_R} & \mathbf{0} \end{bmatrix} \cdot \begin{bmatrix} -\mathbf{I_n} & \mathbf{0} \\ \mathbf{0} & \mathbf{I_p} \end{bmatrix} = \begin{bmatrix} \mathbf{A} & \mathbf{B} \\ -\mathbf{C_R} & \mathbf{0} \end{bmatrix}$$

$$\rho = range \begin{bmatrix} \mathbf{A} & \mathbf{B} \\ -\mathbf{C_R} & \mathbf{0} \end{bmatrix} \tag{2.50}$$

This rank must then have the maximum value $n + q$, which is only possible if $q \leq p$.

Given $\lambda_i = 0$. Then it follows from 2.49 that the last q rows of this matrix are linearly independent of both each other and of the first n rows. Therefore, controllability is sufficiently proved if the first n rows are linearly independent. In other words, that the matrix $\begin{bmatrix} \lambda_i \mathbf{I}_\eta - \mathbf{A} & \mathbf{B} \end{bmatrix}$ has the rank n. According to Hautus' controllability criterion, this holds if the original system $(\mathbf{A}, \mathbf{B})$ is controllable.

It can be stated that this can only be fulfilled if $p \geq q$, i.e. the number of controlled variables is at most equal to the number of control variables.

2.5.4 Static Prefilter

A combination of feedback and feedforward is used to determine the input vector u as seen in figure 2.5. Instead of using the state vector for feedback, the deviation between the projected state $\mathbf{x_s}$ and the current state $\mathbf{x}$ is used [15].

$$\mathbf{e_x} = \mathbf{x_s} - \mathbf{x} \tag{2.51}$$

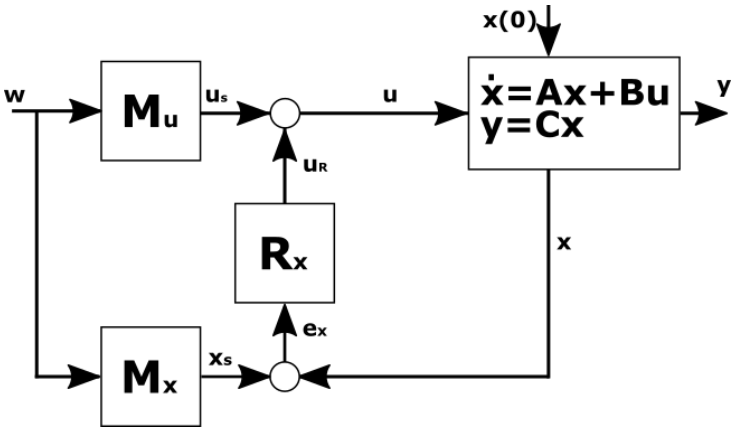

Figure 2.5: Structure of a state control with static feedforward control shown.

This deviation $\mathbf{e_x}$ goes via the regulator R in order to obtain u_R, that will later be added to the first part of the actuator input u_s in order to obtain the full input u [15]. This state control strategy is denoted by

$$\mathbf{u_R} = \mathbf{R}(\mathbf{wM_u} - \mathbf{x}) = \mathbf{R}(\mathbf{x_s} - \mathbf{x}) = \mathbf{R}(\mathbf{e_x}) \tag{2.52}$$
$$\mathbf{u_S} = \mathbf{wM_u} \tag{2.53}$$
$$\mathbf{u} = \mathbf{u_S} + \mathbf{u_R} \tag{2.54}$$

If equations 2.52-2.54 are combined, equation 2.55 can be deduced.

$$\begin{aligned} \mathbf{u} &= \mathbf{wM_u} + \mathbf{R}(\mathbf{wM_u} - \mathbf{x}) \\ &= (\mathbf{M_u} + \mathbf{RM_x})\mathbf{w} - \mathbf{Rx} \end{aligned} \tag{2.55}$$

And if abbreviated so that $\mathbf{M} = \mathbf{M_u} + \mathbf{RM_x}$, results in equation 2.56, represented in figure 2.6.

$$\mathbf{u} = \mathbf{Mw} - \mathbf{Rx} \tag{2.56}$$

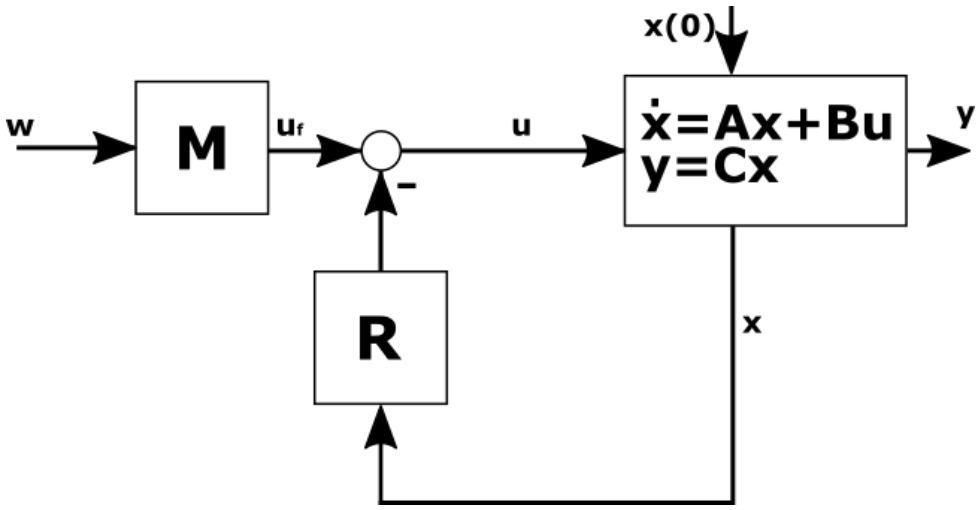

Figure 2.6: Structure of a state control with a state feedback with a prefilter.

Representation as in figure 2.6 is is the most commonly used in control literature. Both structures seen in figures 2.5 and 2.6 behave identically when facing the same inputs $\mathbf{w}$ and $\mathbf{x_0}$. However, the latter misses an actual value comparison that is an essential structural element of control systems. Additionally, the prefilter matrix $\mathbf{M}$ is dependent on the regulator $\mathbf{R}$, while $\mathbf{M_u}$ and $\mathbf{M_x}$ can be designed based on system state equations alone [15].

For calculating the prefilter values, one must consider the equations that result from figure 2.5.

$$
\begin{aligned}
\dot{\mathbf{x}} &= \mathbf{A}\mathbf{x} + \mathbf{B}\mathbf{u} \\
\mathbf{x}(\mathbf{t_0}) &= \mathbf{x_0} \\
\mathbf{y} &= \mathbf{C}\mathbf{x} \\
\mathbf{u} &= \mathbf{u_S} + \mathbf{u_R} \\
\mathbf{u_S} &= \mathbf{M_u}\mathbf{w} \\
\mathbf{u_R} &= \mathbf{R}(\mathbf{x_s} - \mathbf{x}) \\
\mathbf{x_S} &= \mathbf{M_x}\mathbf{w}
\end{aligned}
$$

If it is considered that the guide vector $\mathbf{w}$ aims for a constant stationary value $\mathbf{w}_\infty$ and specific constant setpoint values for the steady state $\mathbf{x_{S\infty}}$ and $\mathbf{u_{S\infty}}$ are defined, the above equations only have to be fulfilled in the steady state [15] and as such simplify into

$$\dot{\mathbf{x}} = 0 = \mathbf{A}\mathbf{x_{S\infty}} + \mathbf{B}\mathbf{u_{S\infty}} \tag{2.57}$$
$$\mathbf{y} = \mathbf{x_{S\infty}} = \mathbf{C}\mathbf{w_{S\infty}} \tag{2.58}$$
$$\mathbf{u} = \mathbf{u_S} + \mathbf{u_R} = \mathbf{u_S} + \mathbf{0} = \mathbf{u_S} \tag{2.59}$$
$$\mathbf{u_S} = \mathbf{M_u}\mathbf{w_{S\infty}} \tag{2.60}$$
$$\mathbf{u_R} = \mathbf{R}(\mathbf{x_{S\infty}} - \mathbf{x_{S\infty}}) = 0 \tag{2.61}$$
$$\mathbf{x_S} = \mathbf{M_x}\mathbf{w_{S\infty}} \tag{2.62}$$

If equations 2.57-2.62 are combined, the following system can be defined.

$$\begin{bmatrix} \mathbf{0} \\ \mathbf{w}_\infty \end{bmatrix} = \begin{bmatrix} \mathbf{A} & \mathbf{B} \\ \mathbf{C} & \mathbf{0} \end{bmatrix} \begin{bmatrix} \mathbf{x_{S\infty}} \\ \mathbf{u_{S\infty}} \end{bmatrix} \tag{2.63}$$
$$\begin{bmatrix} \mathbf{x_{S\infty}} \\ \mathbf{u_{S\infty}} \end{bmatrix} = \begin{bmatrix} \mathbf{M_x} \\ \mathbf{M_u} \end{bmatrix} \mathbf{w}_\infty \tag{2.64}$$

If a q-row identity matrix $\mathbf{I_q}$ is defined and equation 2.64 is introduced in equation 2.63, the equation 2.65 follows, that can only hold for $\mathbf{w}_\infty \neq 0$ if equation 2.66 is true.

$$\begin{bmatrix} \mathbf{0} \\ \mathbf{I_q} \end{bmatrix} w_\infty = \begin{bmatrix} \mathbf{A} & \mathbf{B} \\ \mathbf{C} & \mathbf{0} \end{bmatrix} \begin{bmatrix} \mathbf{M_x} \\ \mathbf{M_u} \end{bmatrix} \mathbf{w}_\infty \tag{2.65}$$
$$\begin{bmatrix} \mathbf{0} \\ \mathbf{I_q} \end{bmatrix} = \begin{bmatrix} \mathbf{A} & \mathbf{B} \\ \mathbf{C} & \mathbf{0} \end{bmatrix} \begin{bmatrix} \mathbf{M_x} \\ \mathbf{M_u} \end{bmatrix} \tag{2.66}$$

If we assume that the number of controlled variables is equal to the number of control variables ($q = p$), the following short-form Rosenbrock system matrix $\mathbf{P}(\mathbf{s})$ seen in equation 2.67 as in equation 2.62 is quadratic, meaning that we can define the Precontrol matrices $\mathbf{M_x}$ and $\mathbf{M_u}$ [15].

$$\mathbf{P}(s) = \begin{bmatrix} \mathbf{A} & \mathbf{B} \\ \mathbf{C} & \mathbf{0} \end{bmatrix} \tag{2.67}$$

$$\begin{bmatrix} \mathbf{M_x} \\ \mathbf{M_u} \end{bmatrix} = \begin{bmatrix} \mathbf{A} & \mathbf{B} \\ \mathbf{C} & \mathbf{0} \end{bmatrix}^{-1} \begin{bmatrix} \mathbf{0} \\ \mathbf{I_q} \end{bmatrix} \tag{2.68}$$

The short-form Rosenbrock system matrix is not always quadratic. When such is the situation, calculating the matrix's inverse is no longer a possibility. In order to be able to proceed under this circumstance, the Moore-Penrose inverse or pseudo-inverse is used instead.

2.5.5 Takagi-Sugeno Static Prefilter

Another alternative is to consider continuous-time dynamic Takagi-Sugeno fuzzy systems [16,17]. The Takagi-Sugeno approach combines a set of linearised models in of a non-linear system in order to approximate it.

Takagi-Sugeno fuzzy models are based on *if-then* rules. The consequent of each rule is a functional expression [17]. The i-th model rule can be described as:

$$\text{If } z_1 \text{ is } Z_1^i \text{ and } ... \text{ and } z_p \text{ is } Z_p^i \text{ then } y = F_i(z)$$

where the vector z has p components z_j for $j = 1, 2, ..., p$, standing as the vector of antecedent or scheduling variables. The sets Z_j^i for $j = 1, 2, ..., p$ and $i = 1, 2, ..., m$, where m is the number of rules, are the antecedent fuzzy sets.

A scheduling variable's value z_j belongs to a fuzzy set Z_j^i with a truth value defined by the membership function $h_{ij} : \mathbb{R} \to [0, 1]$. The truth value for an entire rule is determined on the individual variables, using a conjunction operator such as the minimum or the algebraic product [17].

$$\varphi_i(z) = \min_j \{h_{ij}(z_j)\} \tag{2.69}$$

$$\varphi_i(z) = \prod_{j=1}^{p} h_{ij}(z_j) \tag{2.70}$$

The obtained truth value is then normalized assuming that $\sum_{j=1}^{m} \varphi_j(z) \neq 0$, i.e. for any combination at least one rule has a non-zero truth value [17].

$$\omega_i(z) = \frac{\varphi_i(z)}{\sum_{j=1}^{m} \varphi_j(z)} \tag{2.71}$$

The output of a rule i is the value given by the consequent vector function $\mathbf{F_i}$ and usually depends on the scheduling variables. y is the model's output, computed as the weighted combination

of the rules' output. Using the normalized membership function $w_i(z)$, the model's output is expressed as a function of z as seen in equation 2.72

$$y = \sum_{i=1}^{m} w_i(z)\mathbf{F_i}(z) \tag{2.72}$$

Given a dynamic system as

$$\begin{aligned} \dot{\mathbf{x}} &= \mathbf{f}(\mathbf{x}, \mathbf{u}, \theta) \\ \mathbf{y} &= \mathbf{h}(\mathbf{x}, \zeta) \end{aligned} \tag{2.73}$$

where $\mathbf{f}$ and $\mathbf{h}$ are non-linear functions that represent the state model and the measurement model respectively. $\mathbf{x} \in \mathbb{R}^{n_x}$ is the state vector, $\mathbf{u} \in \mathbb{R}^{n_u}$ is the input vector and $\mathbf{y} \in \mathbb{R}^{n_y}$ is the measurement vector and θ and ζ represent vectors of other constant parameters or exogenous variables that affect the system.

A Takagi-Sugeno fuzzy model for 2.73 is expressed as a set of m rules as seen below, where z_j, $j = 1, 2, ..., p$, represent the scheduling variables and $\hat{\mathbf{f}}_\mathbf{i}$ and $\hat{\mathbf{h}}_\mathbf{i}$ are the consequent functions of the i-th rule.

Model rule i:
If z_1 is Z_1^i and ... and z_p is Z_p^i then
$$\dot{\mathbf{x}} = \hat{\mathbf{f}}_\mathbf{i}(\mathbf{x}, \mathbf{u}, \theta)$$
$$\mathbf{y} = \hat{\mathbf{h}}_\mathbf{i}(\mathbf{x}, \zeta)$$

The scheduling variables are usually chosen as a subset of state, input, output or other variables in the system, or they are functions of these variables. The membership functions $\omega_{ij}(z_j)$ are chosen such that their truth values $\in [0, 1]$ and for any possible value of z at least one of the rules is non-zero. Applying equations 2.70 and 2.72, these can be computed, normalized and combined into

$$\begin{aligned} \dot{\mathbf{x}} &= \frac{\sum_{i=1}^{m} \varphi_i(z)\hat{f}_i(x, u, \theta)}{\sum_{i=1}^{m} \varphi_i(z)} = \sum_{i=1}^{m} \omega_i(z)\hat{f}_i(x, u, \theta) \\ \mathbf{y} &= \frac{\sum_{i=1}^{m} \varphi_i(z)\hat{h}_i(x, \zeta)}{\sum_{i=1}^{m} \varphi_i(z)} = \sum_{i=1}^{m} \omega_i(z)\hat{h}_i(x, \zeta) \end{aligned}$$

The resulting functions $\hat{\mathbf{f}}_\mathbf{i}$ and $\hat{\mathbf{h}}_\mathbf{i}$ are usually less complex that the original non-linear functions $\mathbf{f}$ and $\mathbf{h}$, generally being constant or linear functions. Since these functions are only valid locally,

they can be referred to as "local models". In this thesis, Takagi-Sugeno fuzzy systems are defined with linear local models, which means that the rules have the form seen below.

Model rule i:
If z_1 is Z_1^i and ... and z_p is Z_p^i then
$$\dot{\mathbf{x}} = \mathbf{A_i x} + \mathbf{B_i u}$$
$$\mathbf{y} = \mathbf{C_i x}$$

The computation of the final outputs for the Takagi-Sugeno system are computed as seen in 2.74 below.

$$\begin{aligned} \dot{\mathbf{x}} &= \sum_{i=1}^{m} \omega_{\mathbf{i}}(\mathbf{z})(\mathbf{A_i x} + \mathbf{B_i u}) \\ \mathbf{y} &= \sum_{i=1}^{m} \omega_{\mathbf{i}}(\mathbf{z})\mathbf{C_i x} \end{aligned} \tag{2.74}$$

The normalized membership functions $\omega_i(z)$ make the dynamic Takagi-Sugeno model a convex combination of local linear models, which facilitates the stability analysis of the fuzzy system.

Two main approaches can be used to obtain Takagi-Sugeno fuzzy models. The first one is to identify the model using measured or simulated data, while the other one is to perform an analytic construction of a Takagi-Sugeno model that approximately represents a given non-linear dynamic system.

Since the first approach has so far only been applied to discrete time Takagi-Sugeno models, in this thesis the second approach will be used. Still, there are several methods for constructing a fuzzy representation or approximation of a non-linear system. Linearization in several different operating points is the method used in this thesis. This linearization is a Taylor series expansion in different points of interest, which may or may not be equilibrium points [17].

Considering the dynamic non-linear system

$$\begin{aligned} \dot{\mathbf{x}} &= \mathbf{f}(\mathbf{x}, \mathbf{u}) \\ \mathbf{y} &= \mathbf{h}(\mathbf{x}) \end{aligned} \tag{2.75}$$

where $\mathbf{x} \in \mathbb{R}^{n_x}$ is the state variable vector, $\mathbf{y} \in \mathbb{R}^{n_y}$ is the measurements vector, $\mathbf{u} \in \mathbb{R}^{n_u}$ is the input vector and $\mathbf{f}$ and $\mathbf{h}$ are non-linear vector functions.

An approximation of the non-linear system 2.75, a set of m rules of the form seen below.

Model rule i:

If z_1 is Z_1^i and ... and z_p is Z_p^i then

$$\dot{\mathbf{x}} = \mathbf{A_i}\mathbf{x} + \mathbf{B_i}\mathbf{u} + \mathbf{a_i}$$
$$\mathbf{y} = \mathbf{C_i}\mathbf{x} + \mathbf{c_i}$$

These are equivalent to a Takagi-Sugeno model of the form seen in equation 2.76.

$$\begin{aligned} \dot{\mathbf{x}} &= \sum_{i=1}^{m} \omega_i(z)(\mathbf{A_i}\mathbf{x} + \mathbf{B_i}\mathbf{u} + \mathbf{a_i}) \\ \mathbf{y} &= \sum_{i=1}^{m} \omega_i(z)(\mathbf{C_i}\mathbf{x} + \mathbf{c_i}) \end{aligned} \tag{2.76}$$

where $\mathbf{A_i}, \mathbf{B_i}, \mathbf{a_i}, \mathbf{C_i}$ and $\mathbf{c_i}$ are the matrices and biases of each local linear model, $\mathbf{z}$ is the scheduling vector that determine which rule is active and $\omega_i(\mathbf{z})$, for $i = 1, 2, ..., m$ are the normalized membership functions.

The first step is to define which variables will describe the non-linearity by choosing the scheduling variables. The scheduling vector $\mathbf{z}$ is built as a selection of inputs, states and measurements [17].

Second, a sufficient number m of linearization points $z_{0,i}$ with $i = 1, 2, ..., m$ must be chosen. A partition of the space where the variables are defined and the corresponding memebership functions $h_{ij}(\mathbf{z_j})$ with $i = 1, 2, ..., m$ must also be chosen. The approximation accuracy of the fuzzy model increases when increasing the number of well-chosen approximation points. However, this means that the computational costs of the controller or the observer also increase [17].

Finally, the resulting matrices are

$$\mathbf{A_i} = \left.\frac{\partial f}{\partial x}\right|_{z_{0,i},0}$$
$$\mathbf{A_i} = \left.\frac{\partial f}{\partial u}\right|_{z_{0,i},0}$$
$$\mathbf{C_i} = \left.\frac{\partial h}{\partial x}\right|_{z_{0,i},0}$$

where $|_{z_{0,i},0}$ refers to the evaluation of the expression on the left using the value corresponding to $z_{0,i}$ for the variables that are part of the scheduling vector and 0 for those states and inputs that are not part of it.

Affine terms like a_i and c_i are added because the linearization is not generally done for equilibrium points. These are defined as follows.

$$\begin{aligned} a_i &= \mathbf{f}(\mathbf{x},\mathbf{u})|_{z_{0,i},0} - (\mathbf{A_i x})|_{z_{0,i},0} - (\mathbf{B_i u})|_{z_{0,i},0} \\ c_i &= \mathbf{h}(\mathbf{x})|_{z_{0,i},0} - (\mathbf{C_i x})|_{z_{0,i},0} \end{aligned}$$

In order to define the Takagi-Sugeno system of the form 2.76, the membership functions for each rule are computed with equation 2.70 and normalized using 2.71. It is with the normalized membership functions that the Takagi-Sugeno fuzzy model can be expressed as 2.76.

The stabilization of TakagiSugeno systems via the use of state feedback can be done using various different control laws. In this thesis, linear feedback $\mathbf{u} = -L\mathbf{x}$ as seen in [17] will be used. A Parallel Distributed Compensation scheme as seen in [18] is used, which is composed of linear state feedbacks using the model's non-linear functions.

$$\mathbf{u} = -\sum_{i=1}^{m} w_i(z) L_i \mathbf{x} \tag{2.77}$$

If we introduce equation 2.77 in the model 2.74, the following closed loop results:

$$\begin{aligned} \dot{\mathbf{x}} &= \sum_{i=1}^{m} w_i(z) \left(\mathbf{A_i} - \mathbf{B_i} \sum_{j=1}^{m} w_j(\mathbf{z}) L_j \right) \mathbf{x} \\ &= \sum_{i=1}^{m} w_i(z) \left(\sum_{j=1}^{m} w_j(\mathbf{z}) \mathbf{A_i} - \mathbf{B_i} \sum_{j=1}^{m} w_j(\mathbf{z}) L_j \right) \mathbf{x} \end{aligned} \tag{2.78}$$

Where $\sum_{j=1}^{m} w_j(\mathbf{z})$ before $\mathbf{A_i}$ equals 1. It can be seen that the closed loop is then composed of m^2 linear models.

$$\dot{\mathbf{x}} = \sum_{i=1}^{m} \sum_{j=1}^{m} w_i(\mathbf{z}) w_j(\mathbf{z}) (\mathbf{A_i} - \mathbf{B_i} L_j) \mathbf{x} \tag{2.79}$$

2.6 Least Mean Squares Filter

A simple Least Mean Squares approach is used in this thesis in order to estimate the fundamental harmonic of each phase in the three-phase grid.

The regression equation used in the Least Mean Squares approach is as seen in equation 2.80.

$$\hat{\mathbf{Y}} = \hat{\mathbf{W}}\hat{\mathbf{X}} \tag{2.80}$$

The adaptive filter used to estimate the fundamental harmonic in the k-th step of the estimation loop via the Least Mean Squares approach is as seen in equation 2.81 seen below.

$$\hat{\mathbf{W}}(k+1) = \hat{\mathbf{W}}(k) + \mu\mathbf{e}(k)\hat{\mathbf{X}}^T(k) \tag{2.81}$$

Where μ is the adaptation parameter, which refers to the time needed by the LMS algorithm to learn about its input and reduce the error.

The error vector of the measured and estimated three-phase values is as seen in equation 2.82 seen next.

$$\mathbf{e}(k) = \begin{pmatrix} v_a(k) - \hat{v}_a(k) \\ v_b(k) - \hat{v}_b(k) \\ v_c(k) - \hat{v}_c(k) \end{pmatrix} = \mathbf{Y}(k) - \hat{\mathbf{Y}}(k) \tag{2.82}$$

Chapter 3

Model

3.1 Electrical models

3.1.1 Synchronous Reference Frame

When working on the *abc* frame, some magnitudes present an oscillating nature that complicates the implementation of control systems like the Phase Locked Loop (PLL) or the Current Loop Control (CLC) used in the VSC.

By using the Park transformation and working on the so-called synchronous reference frame it is possible to read this oscillating values as constant quantities [19, 20].

The Park transformation can be defined as the combination of a geometrical transformation that changes the vectors from the standard *abc* reference frame to an ortogonal $\alpha\beta 0$ reference frame (Clarke transformation) and a rotation (θ).

When a balanced three-phase voltage system is considered, the v_0 component of both the $\alpha\beta 0$ and the $qd0$ reference frames is null.

The Park transformation is given by equation 3.1 below.

$$[x_{qd0}] = [T_{qd0}][x_{abc}] \tag{3.1}$$

Where x_{qd0} represents the different magnitudes expressed in the $qd0$ reference frame and x_{abc} the same magnitude in the *abc* frame. The transformation matrix $T_{qd0} = T(\theta)$ and the inverted matrix $T_{qd0}^{-1} = T^{-1}(\theta)$ are defined as follows.

$$T(\theta) = k \begin{bmatrix} cos(\theta) & cos(\theta - \frac{2\pi}{3}) & cos(\theta + \frac{2\pi}{3}) \\ sin(\theta) & sin(\theta - \frac{2\pi}{3}) & sin(\theta + \frac{2\pi}{3}) \\ \frac{1}{2} & \frac{1}{2} & \frac{1}{2} \end{bmatrix} \tag{3.2}$$

$$T^{-1}(\theta) = k \begin{bmatrix} cos(\theta) & sin(\theta) & 1 \\ cos(\theta - \frac{2\pi}{3}) & sin(\theta - \frac{2\pi}{3}) & 1 \\ cos(\theta + \frac{2\pi}{3}) & sin(\theta + \frac{2\pi}{3}) & 1 \end{bmatrix} \tag{3.3}$$

By defining θ as the electrical angle, constant steady state quantities are obtained instead from what once were the oscillating values of voltage and current [19].

Once the studied variables have undergone the needed control procedures, they are reconverted to the *abc* reference frame by means of equation 3.4.

$$[x_{abc}] = [T_{qd0}]^{-1}[x_{qd0}] \tag{3.4}$$

If $k = 2/3$, for balanced sinusoidal conditions, the steady state value of current i_q equals the peak value of i_a [20]. This is why for the rest of this thesis $k = 2/3$ will be assumed.

This can be checked by looking at the expression of i_q and i_d as a function of the currents in the *abc* frame, the angle θ and k in equations 3.5 and 3.6 below. This will be demonstrated with i_q, but it can be applied to i_d too [20]. Given that equations for the individual values of i_q and i_d are being defined, it has been deemed convenient to describe i_0 too, even if it remains unaffected by the constant's value.

$$i_q = k[i_a cos(\theta) + i_b cos(\theta - \frac{2\pi}{3}) + i_c cos(\theta + \frac{2\pi}{3})] \tag{3.5}$$

$$i_d = k[i_a sin(\theta) + i_b sin(\theta - \frac{2\pi}{3}) + i_c sin(\theta + \frac{2\pi}{3})] \tag{3.6}$$

$$i_0 = \frac{1}{3}(i_a + i_b + i_c) \tag{3.7}$$

Equations 3.8-3.10 for i_a, i_b and i_c in balanced conditions have to be substituted into equation 3.5. Doing this results in equation 3.11.

$$i_a = I_m cos(\omega_s t) \tag{3.8}$$

$$i_b = I_m cos(\omega_s t - \frac{2\pi}{3}) \tag{3.9}$$

$$i_c = I_m cos(\omega_s t + \frac{2\pi}{3}) \tag{3.10}$$

$$\begin{aligned} i_q &= k[I_m cos(\omega_s t)cos(\theta) + I_m cos(\omega_s t - \frac{2\pi}{3})cos(\theta - \frac{2\pi}{3}) + I_m cos(\omega_s t + \frac{2\pi}{3})cos(\theta + \frac{2\pi}{3})] \\ &= k\frac{3}{2} I_m cos(\omega_s t - \theta) \end{aligned} \tag{3.11}$$

By substituting $k_d = 2/3$ in equation 3.11, equation 3.12 results, where i_q euqals the peak value I_m of i_a, i_b and i_c in the *abc* frame when the phase θ equals $\omega_s t$.

$$\begin{aligned} i_q &= \frac{2}{3}\frac{3}{2} I_m cos(\omega_s t - \theta) \\ &= I_m cos(\omega_s t - \theta) \end{aligned} \tag{3.12}$$

3.1.2 Voltage Equations

The three phase utility voltages can be described as

$$v_{abcs} = \begin{bmatrix} v_{as} \\ v_{bs} \\ v_{cs} \end{bmatrix} = V_m \cdot \begin{pmatrix} cos\theta \\ cos\left(\theta - \frac{2\pi}{3}\right) \\ cos\left(\theta + \frac{2\pi}{3}\right) \end{pmatrix} \tag{3.13}$$

If balanced utility voltage is assumed, 3.13 can be expressed in the stationary reference frame as

$$v_{\alpha\beta} = \begin{bmatrix} v_{\alpha} \\ v_{\beta} \end{bmatrix} = T_s \cdot v_{abcs} \tag{3.14}$$

Where T_s is the transform matrix

$$T_s = \frac{2}{3} \cdot \begin{pmatrix} 1 & -\frac{1}{2} & -\frac{1}{2} \\ 0 & -\frac{\sqrt{3}}{2} & -\frac{\sqrt{3}}{2} \end{pmatrix} \tag{3.15}$$

These voltage equations can be rewritten in the synchronous reference frame using the PLL output $\hat{\theta}$ as seen below.

$$v_{qde} = \begin{bmatrix} v_{qe} \\ v_{de} \end{bmatrix} = T_e(\hat{\theta}) \cdot v_{\alpha\beta} \tag{3.16}$$

Where $T_e(\hat{\theta})$ is the rotating matrix

$$T_e(\hat{\theta}) = \begin{pmatrix} cos(\hat{\theta}) & -sin(\hat{\theta}) \\ sin(\hat{\theta}) & cos(\hat{\theta}) \end{pmatrix} \tag{3.17}$$

If we group all these equations for doing the transformation from standard to Synchronous Reference Frame, the equation results as follows:

$$v_{qde} = \begin{bmatrix} v_{qe} \\ v_{de} \end{bmatrix} = T_e(\hat{\theta}) \cdot v_{\alpha\beta} = \begin{pmatrix} cos(\hat{\theta}) & -sin(\hat{\theta}) \\ sin(\hat{\theta}) & cos(\hat{\theta}) \end{pmatrix} \cdot v_{\alpha\beta} \tag{3.18}$$

$$= \begin{pmatrix} cos(\hat{\theta}) & -sin(\hat{\theta}) \\ sin(\hat{\theta}) & cos(\hat{\theta}) \end{pmatrix} \cdot T_s \cdot v_{abcs} \tag{3.19}$$

$$= \frac{2}{3} \begin{pmatrix} cos(\hat{\theta}) & -sin(\hat{\theta}) \\ sin(\hat{\theta}) & cos(\hat{\theta}) \end{pmatrix} \cdot \begin{pmatrix} 1 & -\frac{1}{2} & -\frac{1}{2} \\ 0 & -\frac{\sqrt{3}}{2} & -\frac{\sqrt{3}}{2} \end{pmatrix} \cdot v_{abcs} \tag{3.20}$$

$$\begin{pmatrix} v_d \\ v_q \\ v_0 \end{pmatrix} = \frac{2}{3} \begin{pmatrix} cos(\hat{\varphi} - \frac{2\pi}{3}) & cos(\hat{\varphi}) & cos(\hat{\varphi} - \frac{2\pi}{3}) \\ -sin(\hat{\varphi} - \frac{2\pi}{3}) & -sin(\hat{\varphi}) & -sin(\hat{\varphi} - \frac{2\pi}{3}) \\ 0 & 0 & 0 \end{pmatrix} \begin{pmatrix} v_a \\ v_b \\ v_c \end{pmatrix} \tag{3.21}$$

While this would be enough for a balanced system, the point of the thesis is to work with a robust PLL that is able to work in unbalanced systems. As such, it is necessary to also work with the positive sequence components v_x^+, the negative sequence components v_x^- and the zero sequence components v_x^0, with $x = a, b, c$. These are defined as follows:

$$\begin{aligned} v_a &= v_a^+ + v_a^- + v_a^0 \\ v_b &= v_b^+ + v_b^- + v_b^0 \\ v_c &= v_c^+ + v_c^- + v_c^0 \end{aligned} \tag{3.22}$$

Going into further detail, and not taking into account the zero sequence components because the Park transformation yields a zero vector, the symmetrical components are defined as follows:

$$\begin{aligned} v_a^+ &= -V^+ sin(\varphi^+) \\ v_b^+ &= -V^+ sin(\varphi^+ - \frac{2}{3}\pi) \\ v_c^+ &= -V^+ sin(\varphi^+ + \frac{2}{3}\pi) \end{aligned} \tag{3.23}$$

$$\begin{aligned} v_a^- &= -V^- sin(\varphi^- + \varphi_n) \\ v_b^- &= -V^- sin(\varphi^- + \varphi_n + \frac{2}{3}\pi) \\ v_c^- &= -V^- sin(\varphi^- + \varphi_n - \frac{2}{3}\pi) \end{aligned}$$

$$\begin{aligned} \varphi_n &= |\varphi^+| - |\varphi^-| \\ \varphi^- &= -\varphi^+ \end{aligned} \tag{3.24}$$

By substituting 3.23 in 3.22 and then 3.21, 3.25 is obtained.

$$\begin{aligned} v_d &= v_d^+ + v_d^- = -V^+ sin(\Delta\hat{\varphi}^+) + V^- sin(\Delta\hat{\varphi}^+ - \varphi_n) \\ v_q &= v_q^+ - v_q^- = V^+ cos(\Delta\hat{\varphi}^+) - V^- cos(\Delta\hat{\varphi}^+ - \varphi_n) \end{aligned} \tag{3.25}$$

Where $\Delta\hat{\varphi}^+$ is the difference between the reconstructed phase angle φ^+ and the original phase angle $\hat{\varphi}$.

$$\Delta\hat{\varphi}^+ = \varphi^+ - \hat{\varphi} \tag{3.26}$$

If the derivatives of 3.25 are calculated, 3.27 results.

$$\begin{aligned}\dot{v}_d^+ &= -\Delta\hat{\omega}^+ v_q^+ \\ \dot{v}_q^+ &= +\Delta\hat{\omega}^+ v_d^+ \\ \\ \dot{v}_d^- &= -\Delta\hat{\omega}^+ v_q^- \\ \dot{v}_q^- &= +\Delta\hat{\omega}^+ v_d^-\end{aligned} \tag{3.27}$$

3.1.3 Transmission lines

The transmission line is implemented following an RL model. The line impedance Z_{line} [Ω] results as seen in equation 3.28 below.

$$Z_{line} = R_1 + j\omega_s x_1 = R_1 + jL_1 \tag{3.28}$$

3.1.4 Loads

Modelled as a grounded three-phase passive linear branch, an impedance value Z_{load} [Ω] is used to define the load as seen in equation 3.29.

$$Z_{load} = R_{load} + j\omega_s x_{load} = R_{load} + jL_{load} \tag{3.29}$$

3.1.5 Generation

The generation is modelled as a set of three different ideal AC voltage sources whose phase is separated by 120 degrees. The voltage value in p.u. is fed by signal generators that follow the voltage equation seen in section 3.1.2.

3.2 Control Models

3.2.1 State space model

For a model-oriented control design it is necessary to define a state vector $\dot{x}$, an output vector y and an input scalar u as seen below.

$$\mathbf{x} = (\mathbf{x}^+ \ \mathbf{x}^-)^T = (v_d^+ \ v_q^+ \ v_d^- \ v_q^-)^T \tag{3.30}$$

$$\mathbf{y} = \mathbf{x} \tag{3.31}$$

$$\mathbf{u} = \Delta\hat{\omega}^+ \tag{3.32}$$

If said variables are introduced equation 3.27 can be rewritten as:

$$\begin{pmatrix} \dot{x}_1 \\ \dot{x}_2 \\ \dot{x}_3 \\ \dot{x}_4 \end{pmatrix} = \begin{pmatrix} -u\ x_2 \\ +u\ x_1 \\ -u\ x_4 \\ +u\ x_3 \end{pmatrix} \tag{3.33}$$

With this taken into account, the non-linear state space model for the system

$$\dot{\mathbf{x}} = \mathbf{A}\mathbf{x} + \mathbf{B}\mathbf{u}$$
$$\mathbf{y} = \mathbf{C}\mathbf{x} + \mathbf{D}\mathbf{u}$$

can be defined as follows:

$$\mathbf{A} = \begin{pmatrix} 0 & -u & 0 & 0 \\ u & 0 & 0 & 0 \\ 0 & 0 & 0 & -u \\ 0 & 0 & u & 0 \end{pmatrix} \tag{3.34}$$

$$\mathbf{B} = \mathbf{0} \tag{3.35}$$

$$\mathbf{C} = \mathbf{I} = \begin{pmatrix} 1 & 0 & 0 & 0 \\ 0 & 1 & 0 & 0 \\ 0 & 0 & 1 & 0 \\ 0 & 0 & 0 & 1 \end{pmatrix} \tag{3.36}$$

$$\mathbf{D} = \mathbf{0} \tag{3.37}$$

According to Hautus's controllability criteria, as seen on equation 2.50, the resulting system is not controllable. The controllability of the system does not depend on the equilibrium point chosen, since matrix $\mathbf{B}$ is null and therefore ρ can never be maximum.

While not fully controllable, the system is partially controllable. The proof of partial controllability via Kalman decomposition method is out of the scope of this thesis.

3.2.2 I-augmented PLL

In order to define the I-augmented PLL control, a linearised model is required. Given an equilibrium point $\mathbf{x_c}$ and u_c, and applying equations 2.12-2.15 to our model in equation 3.27 and remembering that for the purpose of this thesis $\mathbf{y} = \mathbf{x}$ holds, the following linearised system is obtained.

$$\mathbf{A} = \begin{pmatrix} 0 & -u_c & 0 & 0 \\ u_c & 0 & 0 & 0 \\ 0 & 0 & 0 & -u_c \\ 0 & 0 & u_c & 0 \end{pmatrix} \tag{3.38}$$

$$\mathbf{B} = \begin{pmatrix} -x_{2,c} \\ +x_{1,c} \\ -x_{4,c} \\ +x_{3,c} \end{pmatrix} \tag{3.39}$$

$$\mathbf{C} = \mathbf{I} = \begin{pmatrix} 1 & 0 & 0 & 0 \\ 0 & 1 & 0 & 0 \\ 0 & 0 & 1 & 0 \\ 0 & 0 & 0 & 1 \end{pmatrix} \tag{3.40}$$

$$\mathbf{D} = \mathbf{0} \tag{3.41}$$

Since we are working with a linearized model, the control variables shall be difference variables Δx and Δu as seen next. This also applies to the reference variable Δx_{ref}.

$$\mathbf{\Delta \hat{x}} = \mathbf{\hat{x}} - \mathbf{x_c} = \begin{bmatrix} (\hat{x_1} - x_{1,c}) & (\hat{x_2} - x_{2,c}) & (\hat{x_3} - x_{3,c}) & (\hat{x_4} - x_{4,c}) \end{bmatrix} \tag{3.42}$$

$$\mathbf{\Delta x_{ref}} = \mathbf{x_{ref}} - \mathbf{x_c} = \begin{bmatrix} (x_{1,ref} - x_{1,c}) & (x_{2,ref} - x_{2,c}) & (x_{3,ref} - x_{3,c}) & (x_{4,ref} - x_{4,c}) \end{bmatrix} \tag{3.43}$$

$$\Delta u = u - u_c \tag{3.44}$$

In order to define the gains K_i and K_x, a minimum decay α, a maximum decay β and θ are used to define the region $S_{IAug}(\alpha_{IAug}, \beta_{IAug}, \theta_{IAug})$ where the Regulator is defined through LMI.

For the I-augmented PLL, the conditions seen in equations 2.34 are slightly changed. Poles are forced into real values ($y = 0$) by working with $\theta = 0$. Also, the condition $|x + jy| < r$ is substituted by a maximum decay β as seen in [2]. This results in the conditions seen in equations 3.45:

$$\begin{aligned} x < -\alpha < 0 \\ -\alpha > x \ > -\beta \\ y = 0 \end{aligned} \tag{3.45}$$

A general gain is obtained in the shape of 3.46 which must be divided as integrator gain K_i and feedback gains $\mathbf{K_x}$ separately.

$$\mathbf{K_{IAug}} = \begin{bmatrix} \mathbf{K_x} & -K_i \end{bmatrix} \tag{3.46}$$

$$\mathbf{K_x} = \begin{bmatrix} K_{x,1} & K_{x,2} & K_{x,3} & K_{x,4} \end{bmatrix} \tag{3.47}$$

$$\mathbf{K_i} = \begin{bmatrix} 0 & K_i & 0 & 0 \end{bmatrix} \tag{3.48}$$

The I-augmented PLL obtains the difference input value Δu through the means of equations 3.49-3.52.

$$\Delta u = \Delta u_i - \Delta u_x \tag{3.49}$$

$$\Delta u_i = \frac{\mathbf{K_i}}{s} \cdot \mathbf{\Delta e^T} \tag{3.50}$$

$$\mathbf{\Delta e} = \mathbf{\Delta x_{ref}} - \mathbf{\Delta \hat{x}} \tag{3.51}$$

$$\Delta u_x = \mathbf{K_x} \cdot \mathbf{\Delta x^T} \tag{3.52}$$

By adding the equilibrium point input value u_c to the difference input value Δu obtained we obtain the input value u.

$$u = u_c + \Delta u \tag{3.53}$$

Figure 3.1 below shows a block diagram representing the I-augmented PLL structure.

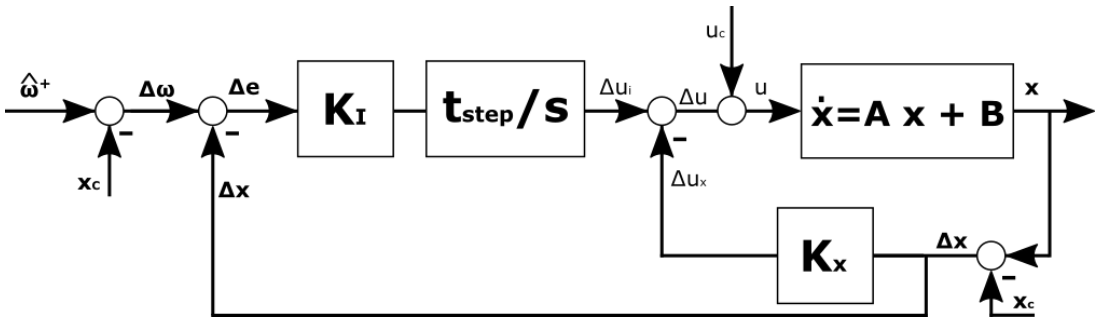

Figure 3.1: Block diagram of the I-augmented PLL.

After $u = \Delta\hat{\omega}^+$ has been obtained, it is necessary to obtain the estimated phase for the positive sequence $\hat{\theta}^+$. The reconstructed frequency $\hat{f}$ is obtained through the means of equation 3.54 below.

$$\hat{f} = f_{ref} \cdot 2\pi - \Delta\hat{\omega}^+ \tag{3.54}$$

This reconstructed frequency $\hat{f}$ is then passed through an integrator as seen in equation 3.55 in order to obtain the estimated phase $\hat{\theta}^+$. Due to the discrete nature of our system, the gain for this integrator will be the time step t_{step} used for the simulations.

$$\hat{\theta}^+ = \hat{f} \cdot \frac{t_{step}}{s} \tag{3.55}$$

The block diagram representation of this part of the process can be seen in figure 3.2.

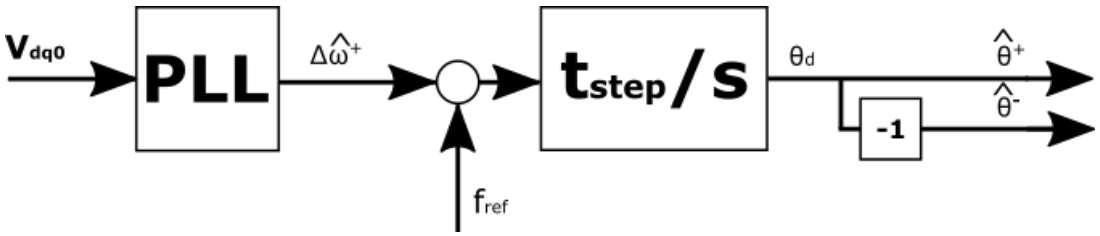

Figure 3.2: Block diagram including the PLL block and the last steps for obtaining the reconstructed phase $\hat{\theta}^+$ for the I-augmented PLL and the Static Prefilter PLL.

3.2.3 Static Prefilter

The linearised model required for the definition of the Static Prefilter control is the same used for the I-augmented PLL in section 3.2.2.

Just like for the I-augmented PLL, the control variables shall be difference variables Δx and Δu. This also applies to the reference variable Δx_{ref}.

$$\begin{aligned}
\mathbf{\Delta x} &= \mathbf{x} - \mathbf{x_c} = \begin{bmatrix}(x_1 - x_{1,c}) & (x_2 - x_{2,c}) & (x_3 - x_{3,c}) & (x_4 - x_{4,c})\end{bmatrix} \\
\mathbf{\Delta x_{ref}} &= \mathbf{x_{ref}} - \mathbf{x_c} = \begin{bmatrix}(x_{1,ref} - x_{1,c}) & (x_{2,ref} - x_{2,c}) & (x_{3,ref} - x_{3,c}) & (x_{4,ref} - x_{4,c})\end{bmatrix} \\
\Delta u &= u - u_c
\end{aligned}$$

In order to define the prefilter gain V and the feedforward gain K, a minimum decay α, a maximum decay β and θ are used to define the region $S_{VFilt}(\alpha_{VFilt}, \beta_{VFilt}, \theta_{VFilt})$ where the Regulator is defined through LMI. For the Static Prefilter PLL region $S_{VFilt}(\alpha_{VFilt}, \beta_{VFilt}, \theta_{VFilt})$, the conditions seen in equations 2.34 apply.

The Static Prefilter PLL obtains the difference input value Δu through the means of equation 3.56.

$$\Delta u = \mathbf{V} \cdot \mathbf{\Delta x_{ref}^T} + \mathbf{K} \cdot \mathbf{\Delta \hat{x}^T} \tag{3.56}$$

By adding the equilibrium point input value u_c to the difference input value Δu obtained we obtain the input value u.

$$u = u_c + \Delta u \tag{3.57}$$

Figure 3.3 below shows a block diagram representing the Static Prefilter PLL structure.

After obtaining $\Delta\hat{\omega}^+ = u$, the process for obtaining $\hat{\theta}^+$ through the Static Prefilter PLL is the same as seen for the I-augmented PLL in equations 3.54, 3.55 and figure 3.2.

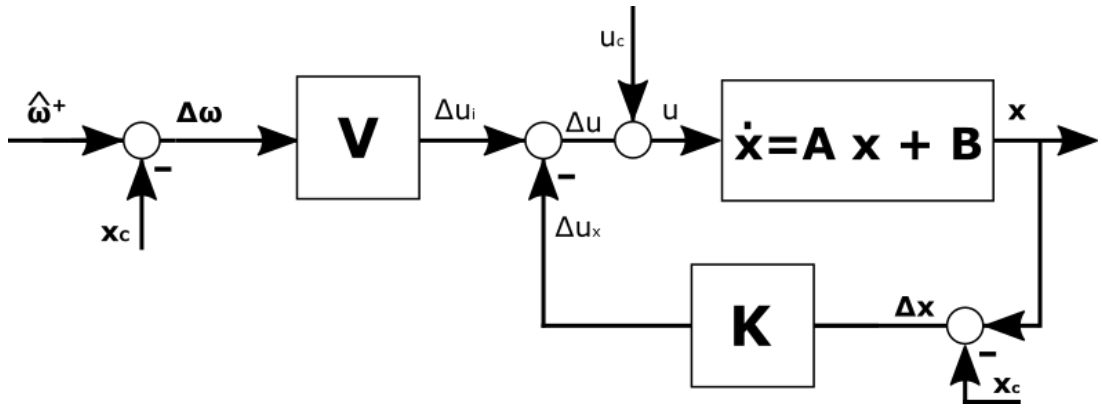

Figure 3.3: Block diagram of Static Prefilter PLL.

3.2.4 Takagi-Sugeno Static Prefilter

While the I-augmented PLL and the Static Prefilter both use the same equilibrium point for their control design, the Takagi-Sugeno Static Prefilter approach requires n different equilibrium points, where n is the number of steps included in the Takagi-Sugeno Static Prefilter control.

For the purpose of this master's thesis, the chosen premise variable z is the frequency deviation $\Delta\hat{\omega}^+ = u$.

$$z = \Delta\hat{\omega}^+ \tag{3.58}$$

Given a minimum frequency f_{min}, a maximum frequency f_{max} and a reference frequency f_{ref}, the equilibrium points $u_{c,i}$ for $i = 1, ..., n$ result as follows.

$$\begin{aligned} u_{c,1} &= 2\pi \cdot (f_{min} - f_{ref}) \\ &\vdots \\ u_{c,i} &= 2\pi \cdot \left(\left(f_{min} + (i) \cdot \tfrac{f_{max} - f_{min}}{n-1} \right) - f_{ref} \right) \\ &\vdots \\ u_{c,n} &= 2\pi \cdot (f_{max} - f_{ref}) \end{aligned} \tag{3.59}$$

A vector $\mathbf{u_c}$ containing the n equilibrium points' $u_{c,i}$ for $i = 1, ..., n$ values as seen below in equation 3.60 is defined.

$$\mathbf{u_c} = \begin{bmatrix} u_{c,1} & \dots & u_{c,i} & \dots & u_{c,n} \end{bmatrix} \tag{3.60}$$

Given the n equilibrium points defined, a membership function $h_i(z)$ for $i = 1, ..., n$ and rules must be defined for each, where z is the premise variable.

The generic membership function defined for the premise variable $z = \Delta\hat{\omega}^+$, which presents minimum value $h_i(z) = 0$ for $z = \Delta\hat{\omega}^+ = a_i, c_i$ and maximum value $h_i(z) = 1$ for $z = \Delta\hat{\omega}^+ = b_i$, is as seen next in equation 3.61:

$$h_i(z) = \begin{cases} 0 & z \leq a_i \\ \frac{z-a_i}{b_i-a_i} & a_i < z \leq b_i \\ \frac{c_i-z}{c_i-b_i} & b_i < z < c_i \\ 0 & c_i \leq z \end{cases} \tag{3.61}$$

These n membership functions $h_i(z)$ are grouped in the vector $\mathbf{h(z)}$.

$$\mathbf{h(z)} = \begin{bmatrix} h_1(z) & \dots & h_i(z) & \dots & h_n(z) \end{bmatrix} \tag{3.62}$$

The equilibrium points referring to the state variables $\mathbf{x}$ are not affected by the premise variable, and as such remain constant and equal to those of the I-augmented PLL and Static Prefilter PLL. The resulting difference variables used are as seen next.

$$\mathbf{\Delta\hat{x}} = \mathbf{\hat{x}} - \mathbf{x_c} = \begin{bmatrix} (\hat{x_1} - x_{1,c}) & (\hat{x_2} - x_{2,c}) & (\hat{x_3} - x_{3,c}) & (\hat{x_4} - x_{4,c}) \end{bmatrix} \tag{3.63}$$

$$\mathbf{\Delta x_{ref}} = \mathbf{x_{ref}} - \mathbf{x_c} = \begin{bmatrix} (x_{1,ref} - x_{1,c}) & (x_{2,ref} - x_{2,c}) & (x_{3,ref} - x_{3,c}) & (x_{4,ref} - x_{4,c}) \end{bmatrix} \tag{3.64}$$

$$\Delta u = u - \mathbf{h(z)} \cdot \mathbf{u_c^T} \tag{3.65}$$

For n equilibrium points, n different linearised models are required. Matrix $\mathbf{A}$ is the only component of the linearised model that is affected by the n different values of the premise variable $\Delta\hat{\omega}^+ = u$, resulting in n different matrices $\mathbf{A}_i$ for $i = 1, ..., n$ as seen in equation 3.66 next.

$$\mathbf{A}_i = \begin{pmatrix} 0 & -u_{c,i} & 0 & 0 \\ u_{c,i} & 0 & 0 & 0 \\ 0 & 0 & 0 & -u_{c,i} \\ 0 & 0 & u_{c,i} & 0 \end{pmatrix} \tag{3.66}$$

Since the equilibrium point $\mathbf{x_c}$ does not vary, all other elements of the linearised model remain unaffected as seen next. If a premise variable that affected these elements of the linearised model were to be chosen, these elements would vary accordingly. For the purpose of this thesis, matrices B, C, D remain constant.

$$\mathbf{B_i} = \mathbf{B} = \begin{pmatrix} -x_{2,c} \\ +x_{1,c} \\ -x_{4,c} \\ +x_{3,c} \end{pmatrix} \tag{3.67}$$

$$\mathbf{C_i} = \mathbf{C} = \mathbf{I} = \begin{pmatrix} 1 & 0 & 0 & 0 \\ 0 & 1 & 0 & 0 \\ 0 & 0 & 1 & 0 \\ 0 & 0 & 0 & 1 \end{pmatrix} \tag{3.68}$$

$$\mathbf{D_i} = \mathbf{D} = \mathbf{0} \tag{3.69}$$

The Takagi-Sugeno Static Prefilter PLL obtains the difference input value Δu through the means of equation 3.70.

$$\Delta u = \mathbf{h(z)} \cdot \mathbf{V} \cdot \Delta x_{ref}^T + \mathbf{h(z)} \cdot \mathbf{K} \cdot \Delta x^T \tag{3.70}$$

Where $\mathbf{V}$ and $\mathbf{K}$ are $[n\,x\,4]$ matrices both including n values of the prefilter gains ($V_{1,i}$, $V_{2,i}$, $V_{3,i}$ and $V_{4,i}$) and the feedforward gains ($K_{1,i}$, $K_{2,i}$, $K_{3,i}$ and $K_{4,i}$) for $i = 1, ..., n$, for each of the four elements of the difference state vector Δx respectively for $i = 1, ..., n$. These vectors are of the form:

$$\mathbf{V} = \begin{bmatrix} V_{1,1} & V_{2,1} & V_{3,1} & V_{4,1} \\ \vdots & \vdots & \vdots & \vdots \\ V_{1,i} & V_{2,i} & V_{3,i} & V_{4,i} \\ \vdots & \vdots & \vdots & \vdots \\ V_{1,n} & V_{2,n} & V_{3,n} & V_{4,n} \end{bmatrix}$$

$$\mathbf{K} = \begin{bmatrix} K_{1,1} & K_{2,1} & K_{3,1} & K_{4,1} \\ \vdots & \vdots & \vdots & \vdots \\ K_{1,i} & K_{2,i} & K_{3,i} & K_{4,i} \\ \vdots & \vdots & \vdots & \vdots \\ K_{1,n} & K_{2,n} & K_{3,n} & K_{4,n} \end{bmatrix}$$

While the calculation of u requires adding the equilibrium point input to the obtained difference input Δu, the Takagi-Sugeno Static Prefilter approach differs in this aspect from the original Static Prefilter PLL since the equilibrium point added depends on the value of the premise variables. The equilibrium point input vector $\mathbf{u_c}$ seen in equation 3.60 is multiplied by the membership function vector $\mathbf{h}(\mathbf{\Delta}\hat{\omega}^+)$ as seen in equation 3.71 next.

$$u = \mathbf{h(z)} \cdot \mathbf{u_c}^T + \Delta u \tag{3.71}$$

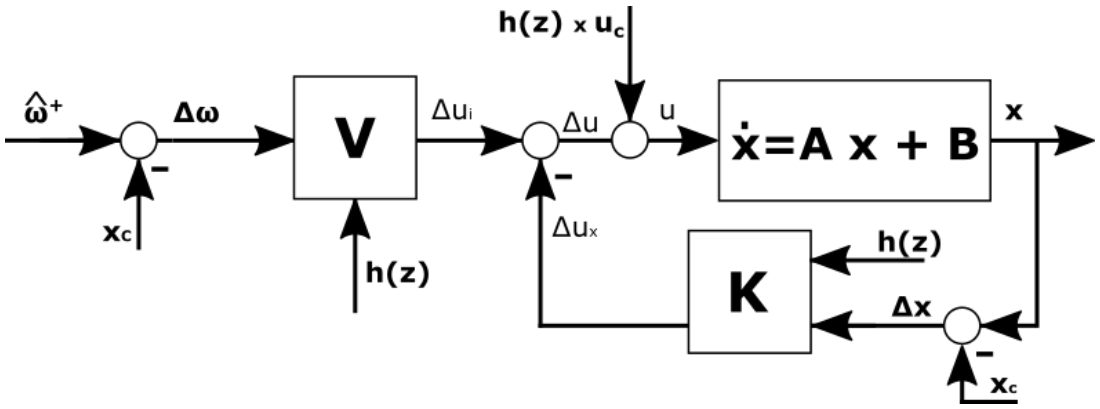

Figure 3.4: Block diagram of Takagi-Sugeno Static Prefilter PLL.

Figure 3.4 below shows a block diagram representing the Takagi-Sugeno Static Prefilter PLL structure.

After $u = \Delta\hat{\omega}^+ = z$ has been obtained, it is necessary to obtain the estimated phase for the positive sequence $\hat{\theta}^+$. The method for the Takagi-Sugeno Prefilter PLL is different from that of the Static Prefilter PLL and the I-augmented PLL, since different equilibrium frequencies $f_{c,i}$ must be defined for each equilibrium point.

For each of the n equilibrium points $u_{c,i}$, an equilibrium frequency $f_{c,i}$ must be defined. This creates an equilibrium frequency vector $\mathbf{f_c}$ composed of each of the frequencies. This vector is obtained by adding f_{ref} to each $u_{c,i}$. Equations 3.72 and 3.73 illustrate this.

$$f_{c,i} = u_{c,i} + f_{ref} \tag{3.72}$$

$$\mathbf{f_c} = \begin{bmatrix} f_{c,1} & \dots & f_{c,i} & \dots & f_{c,n} \end{bmatrix} \tag{3.73}$$

The reconstructed frequency $\hat{f}$ is obtained through the means of equation 3.74 below.

$$\hat{f} = \mathbf{h(z)} \cdot \mathbf{f_c}^T - \Delta\hat{\omega}^+ \tag{3.74}$$

This reconstructed frequency $\hat{f}$ is then passed through an integrator as seen in equation 3.75 in order to obtain the estimated phase $\hat{\theta}^+$. Due to the discrete nature of our system, the gain for this integrator will be the time step t_{step} used for the simulations.

$$\hat{\theta}^+ = \hat{f} \cdot \frac{t_{step}}{s} \tag{3.75}$$

The block diagram representation of this part of the process can be seen in figure 3.5.

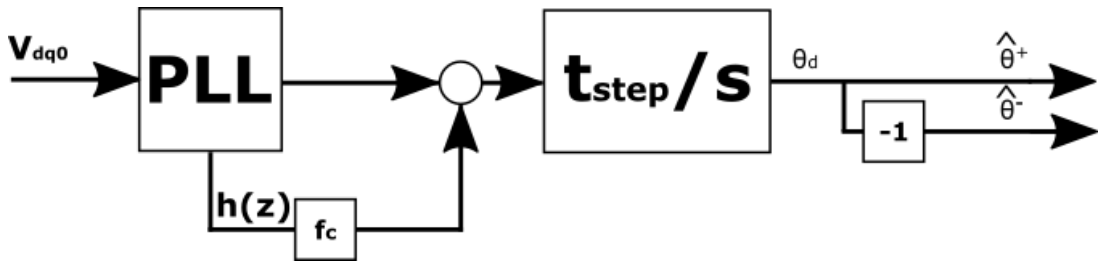

Figure 3.5: Block diagram including the PLL block and the last steps for obtaining the reconstructed phase $\hat{\theta}^{+}$.

Chapter 4

Case

4.1 Electrical environment

The AC ideal voltage sources are set at 1 p.u.

Following equation 3.28 for $R_1 = 0.8929$ $[\Omega]$ and $L_1 = 1.658 \cdot 10^{-2}$ H , the transmission line impedance in the equilibrium point at 50 $[Hz]$ is defined as

$$Z_{line} = 0.8929 + j\,50 \cdot 2\pi \cdot 5.278 \cdot 10^{-5} = 0.8929 + j1.658 \cdot 10^{-2} \tag{4.1}$$

Following equation 3.29 for $R_{load} = 4.2\ \Omega$ and $L_{load} = 1.5 \cdot 10^{-2}$, the load impedance is defined as

$$Z_{load} = 4.2 + j\,50 \cdot 2\pi \cdot 4.775 \cdot 10^{-5} = 4.2 + j1.5 \cdot 10^{-2} \tag{4.2}$$

In figure 4.1 a schematic graphical representation of the electrical model used can be seen. The source point (**SP**) where voltage is 1 p.u., the measure point (**MP**) and the shortcircuit switch (**CC**) have been included for clarity.

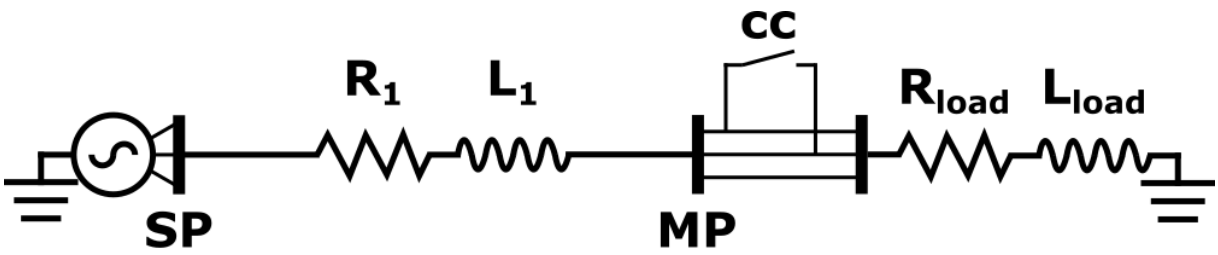

Figure 4.1: Schematic graphical representation of the electrical side of the model used.

4.2 I-augmented PLL

4.2.1 Linearised model

In order to define a linearised model, an equilibrium point $\mathbf{x_c}$ and u_c must first be defined. Ideally, in an equilibrium point should be no need for input, therefore resulting in $u_c = 0$. Our equilibrium point for the state space vector is defined focusing on a grid-synced system, meaning that only the active positive component is considered at a rated value ($1p.u.$).

Equilibrium points result as follows:

$$\mathbf{x_c} = (v_{d,c}^{+}\ v_{q,c}^{+}\ v_{d,c}^{-}\ v_{q,c}^{-})^T = (1\ 0\ 0\ 0)^T \tag{4.3}$$

$$u_c = 0 \tag{4.4}$$

Applying equations 2.12-2.15 to our model in equation 3.27 and remembering that $\mathbf{y} = \mathbf{x}$, the following linearised system is obtained.

$$\mathbf{A} = \begin{pmatrix} 0 & -u_c & 0 & 0 \\ u_c & 0 & 0 & 0 \\ 0 & 0 & 0 & -u_c \\ 0 & 0 & u_c & 0 \end{pmatrix} = \begin{pmatrix} 0 & 0 & 0 & 0 \\ 0 & 0 & 0 & 0 \\ 0 & 0 & 0 & 0 \\ 0 & 0 & 0 & 0 \end{pmatrix} \tag{4.5}$$

$$\mathbf{B} = \begin{pmatrix} -x_{2,c} \\ +x_{1,c} \\ -x_{4,c} \\ +x_{3,c} \end{pmatrix} = \begin{pmatrix} 0 \\ 1 \\ 0 \\ 0 \end{pmatrix} \tag{4.6}$$

$$\mathbf{C} = \mathbf{I} = \begin{pmatrix} 1 & 0 & 0 & 0 \\ 0 & 1 & 0 & 0 \\ 0 & 0 & 1 & 0 \\ 0 & 0 & 0 & 1 \end{pmatrix} \tag{4.7}$$

$$\mathbf{D} = \mathbf{0} \tag{4.8}$$

4.2.2 Control model

For the given equilibrium point, the difference variables result as follows:

$$\begin{aligned} \mathbf{\Delta\hat{x}} = \mathbf{\hat{x}} - \mathbf{x_c} &= \begin{bmatrix} (\hat{x_1} - 0) & (\hat{x_2} - 1) & (\hat{x_3} - 0) & (\hat{x_4} - 0) \end{bmatrix} \\ \mathbf{\Delta x_{ref}} = \mathbf{x_{ref}} - \mathbf{x_c} &= \begin{bmatrix} (x_{1,ref} - 0) & (x_{2,ref} - 1) & (x_{3,ref} - 0) & (x_{4,ref} - 0) \end{bmatrix} \\ \Delta u = u - 0 & \end{aligned}$$

The minimum decay α, maximum decay β and θ used to define the region $S_{IAug}(\alpha_{IAug}, \beta_{IAug}, \theta_{IAug})$ for the I-augmented PLL are as follows.

$$\alpha_{IAug} = 45$$
$$\beta_{IAug} = 259.25$$
$$\theta_{IAug} = 0$$

These parameters result in the region $S_{IAug}(45, 259.25, 0)$ seen in figure 4.2 below.

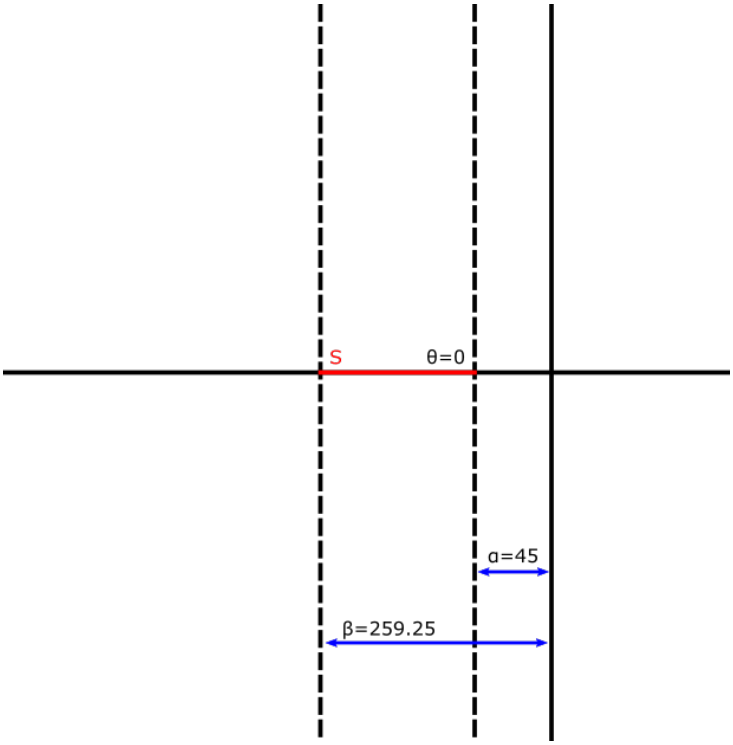

Figure 4.2: Region $S_{IAug}(45, 259.25, 0)$.

Solving the LMI problem limiting the control design to region $S_{IAug}(45, 259.25, 0)$ outputs the following gains.

$$\mathbf{K_{IAug}} = \begin{bmatrix} -0.5961 & 117.4213 & -0.1202 & -0.9295 & -2102.8 \end{bmatrix}$$
$$\mathbf{K_x} = \begin{bmatrix} -0.5961 & 117.4213 & -0.1202 & -0.9295 \end{bmatrix}$$
$$\mathbf{K_i} = \begin{bmatrix} 0 & 2102.8 & 0 & 0 \end{bmatrix}$$

For the K_x and K_i values obtained, equations 3.49-3.52 result as seen next.

$$\Delta u = \Delta u_i - \Delta u_x \tag{4.9}$$

$$\Delta u_i = \frac{\begin{bmatrix}0 & 2102.8 & 0 & 0\end{bmatrix}}{s} \cdot \mathbf{\Delta e^T} \tag{4.10}$$

$$\mathbf{\Delta e} = \mathbf{\Delta x_{ref}} - \mathbf{\Delta \hat{x}} \tag{4.11}$$

$$\Delta u_x = \begin{bmatrix}-0.5961 & 117.4213 & -0.1202 & -0.9295\end{bmatrix} \cdot \mathbf{\Delta x^T} \tag{4.12}$$

Since the equilibrium point input $u_c = 0$, the input value u is equal to the difference input value Δu.

$$u = 0 + \Delta u = \Delta u \tag{4.13}$$

For a reference frequency f_{ref} defined as $50\,Hz$, the reconstructed frequency $\hat{f}$ is obtained through the means of equation 4.14 below.

$$\hat{f} = 50 \cdot 2\pi - \Delta\hat{\omega}^+ \tag{4.14}$$

For a time step $t_{step} = 256 \cdot 10^{-6}\,s$, equation 4.15 below shows the last step for obtaining the reconstructed positive sequence phase $\hat{\theta}^+$.

$$\hat{\theta}^+ = \hat{f} \cdot \frac{256 \cdot 10^{-6}}{s} \tag{4.15}$$

4.3 Static Prefilter

4.3.1 Linearised model

The equilibrium point used for the Static Prefilter is the same than the one used for the I-augmented PLL, resulting in the same linearised model seen in 4.2.1.

Equilibrium points result as follows:

$$\mathbf{x_c} = (v^+_{d,c}\ v^+_{q,c}\ v^-_{d,c}\ v^-_{q,c}) = (1\ 0\ 0\ 0) \tag{4.16}$$

$$u_c = 0 \tag{4.17}$$

The linearised system results as follows:

$$\mathbf{A} = \begin{pmatrix} 0 & -u_c & 0 & 0 \\ u_c & 0 & 0 & 0 \\ 0 & 0 & 0 & -u_c \\ 0 & 0 & u_c & 0 \end{pmatrix} = \begin{pmatrix} 0 & 0 & 0 & 0 \\ 0 & 0 & 0 & 0 \\ 0 & 0 & 0 & 0 \\ 0 & 0 & 0 & 0 \end{pmatrix} \tag{4.18}$$

$$\mathbf{B} = \begin{pmatrix} -x_{2,c} \\ +x_{1,c} \\ -x_{4,c} \\ +x_{3,c} \end{pmatrix} = \begin{pmatrix} 0 \\ 1 \\ 0 \\ 0 \end{pmatrix} \tag{4.19}$$

$$\mathbf{C} = \mathbf{I} = \begin{pmatrix} 1 & 0 & 0 & 0 \\ 0 & 1 & 0 & 0 \\ 0 & 0 & 1 & 0 \\ 0 & 0 & 0 & 1 \end{pmatrix} \tag{4.20}$$

$$\mathbf{D} = \mathbf{0} \tag{4.21}$$

4.3.2 Control model

For the given equilibrium point, the difference variables result as follows:

$$\begin{aligned} \mathbf{\Delta \hat{x}} = \mathbf{\hat{x}} - \mathbf{x_c} &= \begin{bmatrix} (\hat{x_1} - 0) & (\hat{x_2} - 1) & (\hat{x_3} - 0) & (\hat{x_4} - 0) \end{bmatrix} \\ \mathbf{\Delta x_{ref}} = \mathbf{x_{ref}} - \mathbf{x_c} &= \begin{bmatrix} (x_{1,ref} - 0) & (x_{2,ref} - 1) & (x_{3,ref} - 0) & (x_{4,ref} - 0) \end{bmatrix} \\ \Delta u &= u - 0 \end{aligned}$$

The minimum decay α, maximum decay β and θ used to define the region $S_{Vorfilt}(\alpha_{Vorfilt}, \beta_{Vorfilt}, \theta_{Vorfilt})$ for the I-augmented PLL are as follows.

$$\begin{aligned} \alpha_{Vorfilt} &= 45 \\ \beta_{Vorfilt} &= 594.75 \\ \theta_{Vorfilt} &= 0 \end{aligned}$$

These parameters result in the region $S_{Vorfilt}(45, 594.75, 0)$ seen in figure 4.3 below.

Solving the LMI problem limiting the control design to region $S_{Vorfilt}(45, 594.75, 0)$ outputs the following gains.

$$\begin{aligned} \mathbf{V} &= \begin{bmatrix} -31.78 & 95.20 & -31.70 & -31.71 \end{bmatrix} \\ \mathbf{K} &= \begin{bmatrix} -0.02 & 126.97 & 0.05 & 0.04 \end{bmatrix} \end{aligned}$$

For the V and K values obtained, equation 3.56 results as seen next.

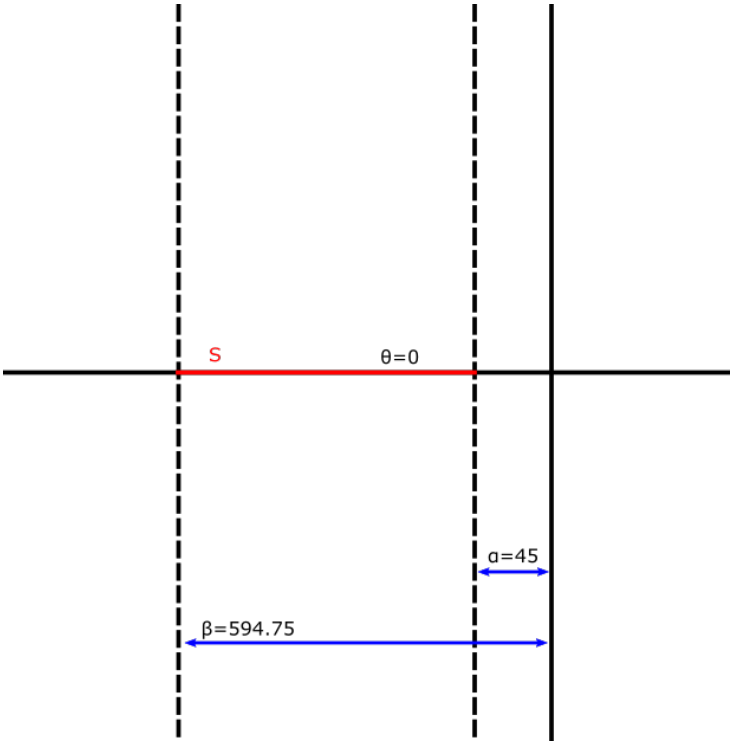

Figure 4.3: Region $S_{Vorfilt}(45, 594.75, 0)$.

$$\Delta u = \begin{bmatrix} -31.78 & 95.20 & -31.70 & -31.71 \end{bmatrix} \cdot \mathbf{\Delta x_{ref}^T} + \begin{bmatrix} -0.02 & 126.97 & 0.05 & 0.04 \end{bmatrix} \cdot \mathbf{\Delta \hat{x}^T} \quad (4.22)$$

Since the equilibrium point input $u_c = 0$, the input value u is equal to the difference input value Δu.

$$u = 0 + \Delta u = \Delta u \quad (4.23)$$

After obtaining $\Delta\hat{\omega}^+ = u$, the process for obtaining $\hat{\theta}^+$ through the Static Prefilter PLL is the same as seen for the I-augmented PLL in equations 4.14 and 4.15.

4.4 Takagi-Sugeno Static Prefilter

4.4.1 Linearised model

As explained before, while the I-augmented PLL and the Static Prefilter both use the same equilibrium point for their control design, the Takagi-Sugeno Static Prefilter approach requires n different equilibrium points, where n is the number of steps included in the Takagi-Sugeno Static Prefilter control. The main TS controller used in this thesis uses $n = 51$ points.

With frequency deviation $\Delta\hat{\omega}^+ = u$ being the chosen premise variable z, frequencies f_{min}, f_{max} and f_{ref} are defined as follows:

$$\begin{aligned} f_{min} &= 45\ Hz = 45 \cdot 2\pi\ \frac{rad}{s} \\ f_{max} &= 55\ Hz = 55 \cdot 2\pi\ \frac{rad}{s} \\ f_{ref} &= 50\ Hz = 50 \cdot 2\pi\ \frac{rad}{s} \end{aligned}$$

With these frequency values, the resulting equilibrium points $u_{c,i}$ for $i = 1, ..., 51$ are as follows.

$$\begin{aligned} u_{c,1} &= 2\pi \cdot (45 - 50) = -5 \cdot 2\pi \\ &\vdots \\ u_{c,i} &= 2\pi \cdot \left(\left(45 + (i-1) \cdot \tfrac{55-45}{10}\right) - 50\right) \\ &\vdots \\ u_{c,51} &= 2\pi \cdot (55 - 50) = +5 \cdot 2\pi \end{aligned} \tag{4.24}$$

A vector $\mathbf{u_c}$ containing the $n = 51$ equilibrium points' $u_{c,i}$ for $i = 1, ..., 51$ values as seen below in equation 4.25 is defined.

$$\mathbf{u_c} = \begin{bmatrix} 45.0 & 45.2 & 45.4 & \dots & u_{c,i} & \dots & 54.6 & 54.8 & 55.0 \end{bmatrix} \tag{4.25}$$

The equilibrium and reference points referring to the state variables $\mathbf{x}$ are not affected by the premise variable, and as such remain constant and equal to those of the I-augmented PLL and Static Prefilter PLL.

$$\begin{aligned} \mathbf{x_c} &= \begin{bmatrix} 1 & 0 & 0 & 0 \end{bmatrix} \\ \mathbf{x_{ref}} &= \begin{bmatrix} 1 & 0 & 0 & 0 \end{bmatrix} \end{aligned}$$

For n equilibrium points, n different linearised models are required. Matrix $\mathbf{A}$ is the only component of the linearised model that is affected by the n different values of the premise variable $\Delta\hat{\omega}^+ = u = z$, resulting in n different matrices $\mathbf{A}_i$ for $i = 1, ..., n$ as seen in equation 4.26 next.

$$
\begin{aligned}
\mathbf{A}_1 &= \begin{pmatrix} 0 & 5\cdot 2\pi & 0 & 0 \\ -5\cdot 2\pi & 0 & 0 & 0 \\ 0 & 0 & 0 & 5\cdot 2\pi \\ 0 & 0 & -5\cdot 2\pi & 0 \end{pmatrix} \\
&\vdots \\
\mathbf{A}_i &= \begin{pmatrix} 0 & -u_{c,i} & 0 & 0 \\ u_{c,i} & 0 & 0 & 0 \\ 0 & 0 & 0 & -u_{c,i} \\ 0 & 0 & u_{c,i} & 0 \end{pmatrix} \\
&\vdots \\
\mathbf{A}_{51} &= \begin{pmatrix} 0 & -5\cdot 2\pi & 0 & 0 \\ 5\cdot 2\pi & 0 & 0 & 0 \\ 0 & 0 & 0 & -5\cdot 2\pi \\ 0 & 0 & 5\cdot 2\pi & 0 \end{pmatrix}
\end{aligned} \tag{4.26}
$$

A list with all the values that $u_{c,i}$ takes can be seen in table 4.1.

Since the equilibrium point $\mathbf{x_c}$ does not vary, all other elements of the linearised model remain unaffected as seen next. If a premise variable that affected these elements of the linearised model were to be chosen, these elements would vary accordingly. For the purpose of this thesis, matrices B, C, D remain constant.

$$
\mathbf{B_i} = \mathbf{B} = \begin{pmatrix} -x_{2,c} \\ +x_{1,c} \\ -x_{4,c} \\ +x_{3,c} \end{pmatrix}
$$

$$
\mathbf{C_i} = \mathbf{C} = \mathbf{I} = \begin{pmatrix} 1 & 0 & 0 & 0 \\ 0 & 1 & 0 & 0 \\ 0 & 0 & 1 & 0 \\ 0 & 0 & 0 & 1 \end{pmatrix}
$$

$$
\mathbf{D_i} = \mathbf{D} = \mathbf{0}
$$

4.4.2 Control model

The minimum decay α, maximum decay β and θ used to define the region $S_{TS}(\alpha_{TS}, \beta_{TS}, \theta_{TS})$ for the Takagi-Sugeno Static Prefilter PLL are as follows.

$$
\begin{aligned}
\alpha_{TS} &= 120 \\
\beta_{TS} &= 315 \\
\theta_{TS} &= 60
\end{aligned}
$$

These parameters result in the region $S_{TS}(120, 315, 60)$ seen in figure 4.4 below.

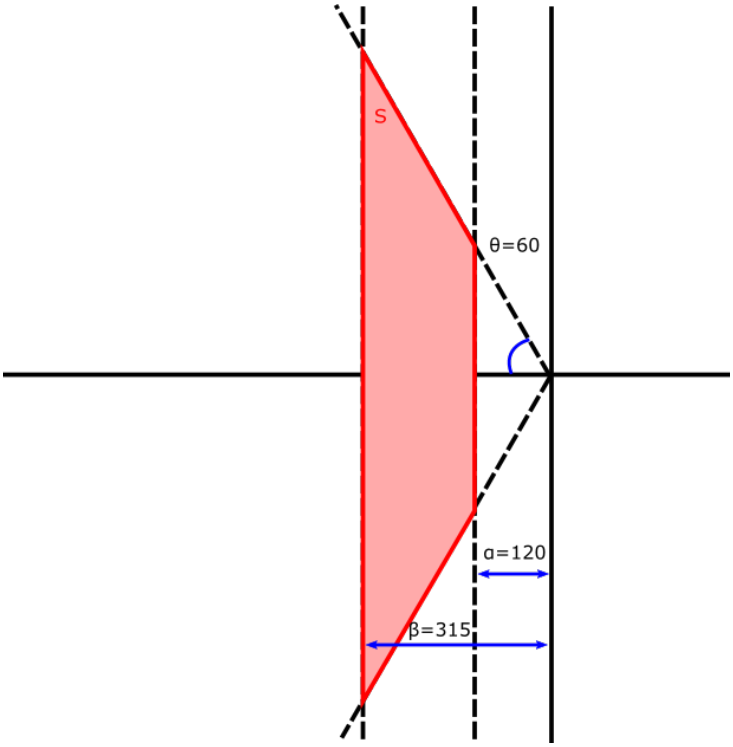

Figure 4.4: Region $S_{TS}(120, 315, 60)$.

For the given equilibrium points, the resulting difference variables used are as seen next.

$$\begin{aligned}
\mathbf{\Delta\hat{x}} &= \hat{x} - x_c = \begin{bmatrix}(\hat{x_1} - 1) & (\hat{x_2} - 0) & (\hat{x_3} - 0) & (\hat{x_4} - 0)\end{bmatrix} \\
\mathbf{\Delta x_{ref}} &= \mathbf{x_{ref}} - \mathbf{x_c} = \begin{bmatrix}(1 - 1) & (0 - 0) & (0 - 0) & (0 - 0)\end{bmatrix} = \begin{bmatrix}0 & 0 & 0 & 0\end{bmatrix} \\
\Delta u &= u - \mathbf{h(z)} \cdot \mathbf{u_c^T}
\end{aligned}$$

The $n = 51$ membership functions $h_i(z)$ for $i = 1, ..., 51$ that compose the membership function vector $\mathbf{h(z)}$ are defined following equation 3.61. In tables 4.1 and 4.2 below, the equilibrium points $u_{c,i}$, corresponding equilibrium frequency $f_{c,i}$ and membership function parameters a_i, b_i and c_i for each of the $n = 51$ equilibrium points used are shown.

Obtained through solving the LMI problem, the gain values for the matrices $\mathbf{V}$ and $\mathbf{K}$ used in the Takagi-Sugeno Static Prefilter PLL for obtaining the difference input value Δu through the means of equation 3.70.

The $\mathbf{V}$ and $\mathbf{K}$ are $[n\,x\,4]$ matrices including the $n = 51$ values of the prefilter gains ($V_{1,i}$, $V_{2,i}$, $V_{3,i}$ and $V_{4,i}$) and the feedforward gains ($K_{1,i}$, $K_{2,i}$, $K_{3,i}$ and $K_{4,i}$) for $i = 1, ..., 51$ are of the form:

$$\mathbf{V} = \begin{bmatrix} V_{1,1} & V_{2,1} & V_{3,1} & V_{4,1} \\ \vdots & \vdots & \vdots & \vdots \\ V_{1,i} & V_{2,i} & V_{3,i} & V_{4,i} \\ \vdots & \vdots & \vdots & \vdots \\ V_{1,51} & V_{2,51} & V_{3,51} & V_{4,51} \end{bmatrix}$$

$$\mathbf{K} = \begin{bmatrix} K_{1,1} & K_{2,1} & K_{3,1} & K_{4,1} \\ \vdots & \vdots & \vdots & \vdots \\ K_{1,i} & K_{2,i} & K_{3,i} & K_{4,i} \\ \vdots & \vdots & \vdots & \vdots \\ K_{1,51} & K_{2,51} & K_{3,51} & K_{4,51} \end{bmatrix}$$

Feedforward gains $\mathbf{K}$ are shown in tables 4.3 and 4.4, and prefilter gains $\mathbf{V}$ are shown in tables 4.5 and 4.6. These tables can be found at the end of this section.

With the defined gains $\mathbf{K}$ and $\mathbf{V}$ from tables 4.3, 4.4, 4.5 and 4.6 respectively, equilibrium points $\mathbf{u_c}$ and $\mathbf{f_c}$ and membership functions $\mathbf{h(z)}$ from table 4.1 and reference points, all necessary elements for the calculation of $\Delta\hat{\omega}^+$ are present.

$$\Delta u = \mathbf{h(z)} \cdot \mathbf{V} \cdot \Delta x_{ref}^T + \mathbf{h(z)} \cdot \mathbf{K} \cdot \Delta x^T$$

In order to calculate u for the Takagi-Sugeno Static Prefilter approach, the equilibrium point input vector $\mathbf{u_c}$ seen in equation 4.25 is multiplied by the membership function vector $\mathbf{h(z)}$ as seen in equation 3.71.

$$u = \mathbf{h(z)} \cdot \mathbf{u_c}^T + \Delta u$$

Obtaining the estimated phase for the positive sequence $\hat{\theta}^+$ after $\Delta\hat{\omega}^+ = u$ has been obtained requires the equilibrium frequencies from table 4.1. The reconstructed frequency $\hat{f}$ is obtained through the means of equation 3.74.

$$\begin{aligned} f_{c,i} &= u_{c,i} + 50 \\ \hat{f} &= \mathbf{h(z)} \cdot \mathbf{f_c}^T - \Delta\hat{\omega}^+ \end{aligned}$$

This reconstructed frequency $\hat{f}$ is then passed through an integrator as seen in equation 3.75 in order to obtain the estimated phase $\hat{\theta}^+$. The time step t_{step} used as integrator gain due to the discrete nature of our system is the same used for the I-augmented PLL and the Static Prefilter PLL, $t_{step} = 256 \cdot 10^{-6}\, s$.

$$\hat{\theta}^{+} = \hat{f} \cdot \frac{256 \cdot 10^{-6}}{s} \tag{4.27}$$

In figure 4.5 the result of the pole positioning can be seen. Since the system is not fully controllable, the poles pertaining to the non-controllable portion of the system are not inside the $S_{TS}(\alpha_{TS}, \beta_{TS}, \theta_{TS})$ region defined.

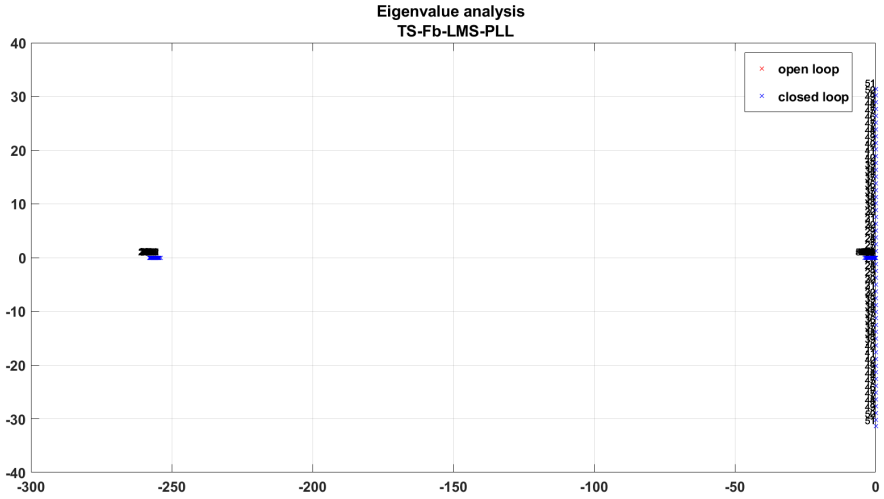

Figure 4.5: Eigenvalue analysis of the TS Static Prefilter.

Table 4.1: Equilibrium points $u_{c,i}$, corresponding equilibrium frequency $f_{c,i}$ and membership function parameters a_i, b_i and c_i $(i = 1, ..., 26)$.

i	$u_{c,i}$	$f_{c,i}$	a_i	b_i	c_i
1	$-5.0 \cdot 2\pi$	$45.0 \cdot 2\pi$	$44.8 \cdot 2\pi$	$45.0 \cdot 2\pi$	$45.2 \cdot 2\pi$
2	$-4.8 \cdot 2\pi$	$45.2 \cdot 2\pi$	$45.0 \cdot 2\pi$	$45.2 \cdot 2\pi$	$45.4 \cdot 2\pi$
3	$-4.6 \cdot 2\pi$	$45.4 \cdot 2\pi$	$45.2 \cdot 2\pi$	$45.4 \cdot 2\pi$	$45.6 \cdot 2\pi$
4	$-4.4 \cdot 2\pi$	$45.6 \cdot 2\pi$	$45.4 \cdot 2\pi$	$45.6 \cdot 2\pi$	$45.8 \cdot 2\pi$
5	$-4.2 \cdot 2\pi$	$45.8 \cdot 2\pi$	$45.6 \cdot 2\pi$	$45.8 \cdot 2\pi$	$46.0 \cdot 2\pi$
6	$-4.0 \cdot 2\pi$	$46.0 \cdot 2\pi$	$45.8 \cdot 2\pi$	$46.0 \cdot 2\pi$	$46.2 \cdot 2\pi$
7	$-3.8 \cdot 2\pi$	$46.2 \cdot 2\pi$	$46.0 \cdot 2\pi$	$46.2 \cdot 2\pi$	$46.4 \cdot 2\pi$
8	$-3.6 \cdot 2\pi$	$46.4 \cdot 2\pi$	$46.2 \cdot 2\pi$	$46.4 \cdot 2\pi$	$46.6 \cdot 2\pi$
9	$-3.4 \cdot 2\pi$	$46.6 \cdot 2\pi$	$46.4 \cdot 2\pi$	$46.6 \cdot 2\pi$	$46.8 \cdot 2\pi$
10	$-3.2 \cdot 2\pi$	$46.8 \cdot 2\pi$	$46.6 \cdot 2\pi$	$46.8 \cdot 2\pi$	$47.0 \cdot 2\pi$
11	$-3.0 \cdot 2\pi$	$47.0 \cdot 2\pi$	$46.8 \cdot 2\pi$	$47.0 \cdot 2\pi$	$47.2 \cdot 2\pi$
12	$-2.8 \cdot 2\pi$	$47.2 \cdot 2\pi$	$47.0 \cdot 2\pi$	$47.2 \cdot 2\pi$	$47.4 \cdot 2\pi$
13	$-2.6 \cdot 2\pi$	$47.4 \cdot 2\pi$	$47.2 \cdot 2\pi$	$47.4 \cdot 2\pi$	$47.6 \cdot 2\pi$
14	$-2.4 \cdot 2\pi$	$47.6 \cdot 2\pi$	$47.4 \cdot 2\pi$	$47.6 \cdot 2\pi$	$47.8 \cdot 2\pi$
15	$-2.2 \cdot 2\pi$	$47.8 \cdot 2\pi$	$47.6 \cdot 2\pi$	$47.8 \cdot 2\pi$	$48.0 \cdot 2\pi$
16	$-2.0 \cdot 2\pi$	$48.0 \cdot 2\pi$	$47.8 \cdot 2\pi$	$48.0 \cdot 2\pi$	$48.2 \cdot 2\pi$
17	$-1.8 \cdot 2\pi$	$48.2 \cdot 2\pi$	$48.0 \cdot 2\pi$	$48.2 \cdot 2\pi$	$48.4 \cdot 2\pi$
18	$-1.6 \cdot 2\pi$	$48.4 \cdot 2\pi$	$48.2 \cdot 2\pi$	$48.4 \cdot 2\pi$	$48.6 \cdot 2\pi$
19	$-1.4 \cdot 2\pi$	$48.6 \cdot 2\pi$	$48.4 \cdot 2\pi$	$48.6 \cdot 2\pi$	$48.8 \cdot 2\pi$
20	$-1.2 \cdot 2\pi$	$48.8 \cdot 2\pi$	$48.6 \cdot 2\pi$	$48.8 \cdot 2\pi$	$49.0 \cdot 2\pi$
21	$-1.0 \cdot 2\pi$	$49.0 \cdot 2\pi$	$48.8 \cdot 2\pi$	$49.0 \cdot 2\pi$	$49.2 \cdot 2\pi$
22	$-0.8 \cdot 2\pi$	$49.2 \cdot 2\pi$	$49.0 \cdot 2\pi$	$49.2 \cdot 2\pi$	$49.4 \cdot 2\pi$
23	$-0.6 \cdot 2\pi$	$49.4 \cdot 2\pi$	$49.2 \cdot 2\pi$	$49.4 \cdot 2\pi$	$49.6 \cdot 2\pi$
24	$-0.4 \cdot 2\pi$	$49.6 \cdot 2\pi$	$49.4 \cdot 2\pi$	$49.6 \cdot 2\pi$	$49.8 \cdot 2\pi$
25	$-0.2 \cdot 2\pi$	$49.8 \cdot 2\pi$	$49.6 \cdot 2\pi$	$49.8 \cdot 2\pi$	$50.0 \cdot 2\pi$
26	$\pm 0.0 \cdot 2\pi$	$50.0 \cdot 2\pi$	$49.8 \cdot 2\pi$	$50.0 \cdot 2\pi$	$50.2 \cdot 2\pi$

Table 4.2: Equilibrium points $u_{c,i}$, corresponding equilibrium frequency $f_{c,i}$ and membership function parameters a_i, b_i and c_i $(i = 27, ..., 51)$.

i	$u_{c,i}$	$f_{c,i}$	a_i	b_i	c_i
27	$+0.2 \cdot 2\pi$	$50.2 \cdot 2\pi$	$50.0 \cdot 2\pi$	$50.2 \cdot 2\pi$	$50.4 \cdot 2\pi$
28	$+0.4 \cdot 2\pi$	$50.4 \cdot 2\pi$	$50.2 \cdot 2\pi$	$50.4 \cdot 2\pi$	$50.6 \cdot 2\pi$
29	$+0.6 \cdot 2\pi$	$50.6 \cdot 2\pi$	$50.4 \cdot 2\pi$	$50.6 \cdot 2\pi$	$50.8 \cdot 2\pi$
30	$+0.8 \cdot 2\pi$	$50.8 \cdot 2\pi$	$50.6 \cdot 2\pi$	$50.8 \cdot 2\pi$	$51.0 \cdot 2\pi$
31	$+1.0 \cdot 2\pi$	$51.0 \cdot 2\pi$	$50.8 \cdot 2\pi$	$51.0 \cdot 2\pi$	$51.2 \cdot 2\pi$
32	$+1.2 \cdot 2\pi$	$51.2 \cdot 2\pi$	$51.0 \cdot 2\pi$	$51.2 \cdot 2\pi$	$51.4 \cdot 2\pi$
33	$+1.4 \cdot 2\pi$	$51.4 \cdot 2\pi$	$51.2 \cdot 2\pi$	$51.4 \cdot 2\pi$	$51.6 \cdot 2\pi$
34	$+1.6 \cdot 2\pi$	$51.6 \cdot 2\pi$	$51.4 \cdot 2\pi$	$51.6 \cdot 2\pi$	$51.8 \cdot 2\pi$
35	$+1.8 \cdot 2\pi$	$51.8 \cdot 2\pi$	$51.6 \cdot 2\pi$	$51.8 \cdot 2\pi$	$52.0 \cdot 2\pi$
36	$+2.0 \cdot 2\pi$	$52.0 \cdot 2\pi$	$51.8 \cdot 2\pi$	$52.0 \cdot 2\pi$	$52.2 \cdot 2\pi$
37	$+2.2 \cdot 2\pi$	$52.2 \cdot 2\pi$	$52.0 \cdot 2\pi$	$52.2 \cdot 2\pi$	$52.4 \cdot 2\pi$
38	$+2.4 \cdot 2\pi$	$52.4 \cdot 2\pi$	$52.2 \cdot 2\pi$	$52.4 \cdot 2\pi$	$52.6 \cdot 2\pi$
39	$+2.6 \cdot 2\pi$	$52.6 \cdot 2\pi$	$52.4 \cdot 2\pi$	$52.6 \cdot 2\pi$	$52.8 \cdot 2\pi$
40	$+2.8 \cdot 2\pi$	$52.8 \cdot 2\pi$	$52.6 \cdot 2\pi$	$52.8 \cdot 2\pi$	$53.0 \cdot 2\pi$
41	$+3.0 \cdot 2\pi$	$53.0 \cdot 2\pi$	$52.8 \cdot 2\pi$	$53.0 \cdot 2\pi$	$53.2 \cdot 2\pi$
42	$+3.2 \cdot 2\pi$	$53.2 \cdot 2\pi$	$53.0 \cdot 2\pi$	$53.2 \cdot 2\pi$	$53.4 \cdot 2\pi$
43	$+3.4 \cdot 2\pi$	$53.4 \cdot 2\pi$	$53.2 \cdot 2\pi$	$53.4 \cdot 2\pi$	$53.6 \cdot 2\pi$
44	$+3.6 \cdot 2\pi$	$53.6 \cdot 2\pi$	$53.4 \cdot 2\pi$	$53.6 \cdot 2\pi$	$53.8 \cdot 2\pi$
45	$+3.8 \cdot 2\pi$	$53.8 \cdot 2\pi$	$53.6 \cdot 2\pi$	$53.8 \cdot 2\pi$	$54.0 \cdot 2\pi$
46	$+4.0 \cdot 2\pi$	$54.0 \cdot 2\pi$	$53.8 \cdot 2\pi$	$54.0 \cdot 2\pi$	$54.2 \cdot 2\pi$
47	$+4.2 \cdot 2\pi$	$54.2 \cdot 2\pi$	$54.0 \cdot 2\pi$	$54.2 \cdot 2\pi$	$54.4 \cdot 2\pi$
48	$+4.4 \cdot 2\pi$	$54.4 \cdot 2\pi$	$54.2 \cdot 2\pi$	$54.4 \cdot 2\pi$	$54.6 \cdot 2\pi$
49	$+4.6 \cdot 2\pi$	$54.6 \cdot 2\pi$	$54.4 \cdot 2\pi$	$54.6 \cdot 2\pi$	$54.8 \cdot 2\pi$
50	$+4.8 \cdot 2\pi$	$54.8 \cdot 2\pi$	$54.6 \cdot 2\pi$	$54.8 \cdot 2\pi$	$49.8 \cdot 2\pi$
51	$+5.0 \cdot 2\pi$	$55.0 \cdot 2\pi$	$54.8 \cdot 2\pi$	$55.0 \cdot 2\pi$	$55.2 \cdot 2\pi$

Table 4.3: Equilibrium points $u_{c,i}$ and corresponding feedforward gain values $\mathbf{K}$ ($i = 1, ..., 26$).

i	$u_{c,i}$	$K_{1,i}$	$K_{2,i}$	$K_{3,i}$	$K_{4,i}$
1	$-5.0 \cdot 2\pi$	000.4435	257.9350	002.7767	000.9534
2	$-4.8 \cdot 2\pi$	000.3525	257.9724	003.1331	001.4699
3	$-4.6 \cdot 2\pi$	000.3525	257.9724	003.1331	001.4699
4	$-4.4 \cdot 2\pi$	000.3525	257.9724	003.1331	001.4699
5	$-4.2 \cdot 2\pi$	000.3525	257.9724	003.1331	001.4699
6	$-4.0 \cdot 2\pi$	000.3525	257.9724	003.1331	001.4699
7	$-3.8 \cdot 2\pi$	000.3525	257.9724	003.1331	001.4699
8	$-3.6 \cdot 2\pi$	000.3525	257.9724	003.1331	001.4699
9	$-3.4 \cdot 2\pi$	000.3525	257.9724	003.1331	001.4699
10	$-3.2 \cdot 2\pi$	001.0021	258.0043	002.7945	001.1608
11	$-3.0 \cdot 2\pi$	000.3525	257.9724	003.1331	001.4699
12	$-2.8 \cdot 2\pi$	000.3525	257.9724	003.1331	001.4699
13	$-2.6 \cdot 2\pi$	000.3525	257.9724	003.1331	001.4699
14	$-2.4 \cdot 2\pi$	000.3525	257.9724	003.1331	001.4699
15	$-2.2 \cdot 2\pi$	000.3525	257.9724	003.1331	001.4699
16	$-2.0 \cdot 2\pi$	000.3525	257.9724	003.1331	001.4699
17	$-1.8 \cdot 2\pi$	000.3525	257.9724	003.1331	001.4699
18	$-1.6 \cdot 2\pi$	000.3525	257.9724	003.1331	001.4699
19	$-1.4 \cdot 2\pi$	000.3525	257.9724	003.1331	001.4699
20	$-1.2 \cdot 2\pi$	000.3525	257.9724	003.1331	001.4699
21	$-1.0 \cdot 2\pi$	000.3525	257.9724	003.1331	001.4699
22	$-0.8 \cdot 2\pi$	000.3525	257.9724	003.1331	001.4699
23	$-0.6 \cdot 2\pi$	000.3525	257.9724	003.1331	001.4699
24	$-0.4 \cdot 2\pi$	000.3525	257.9724	003.1331	001.4699
25	$-0.2 \cdot 2\pi$	000.3525	257.9724	003.1331	001.4699
26	$\pm 0.0 \cdot 2\pi$	000.3525	257.9724	003.1331	001.4699

Table 4.4: Equilibrium points $u_{c,i}$ and corresponding feedforward gain values $\mathbf{K}$ ($i = 27, ..., 51$).

i	$u_{c,i}$	$K_{1,i}$	$K_{2,i}$	$K_{3,i}$	$K_{4,i}$
27	$+0.2 \cdot 2\pi$	000.3525	257.9724	003.1331	001.4699
28	$+0.4 \cdot 2\pi$	000.3525	257.9724	003.1331	001.4699
29	$+0.6 \cdot 2\pi$	000.3525	257.9724	003.1331	001.4699
30	$+0.8 \cdot 2\pi$	000.3525	257.9724	003.1331	001.4699
31	$+1.0 \cdot 2\pi$	000.3525	257.9724	003.1331	001.4699
32	$+1.2 \cdot 2\pi$	000.3525	257.9724	003.1331	001.4699
33	$+1.4 \cdot 2\pi$	000.3525	257.9724	003.1331	001.4699
34	$+1.6 \cdot 2\pi$	000.3525	257.9724	003.1331	001.4699
35	$+1.8 \cdot 2\pi$	000.3525	257.9724	003.1331	001.4699
36	$+2.0 \cdot 2\pi$	000.3525	257.9724	003.1331	001.4699
37	$+2.2 \cdot 2\pi$	000.3525	257.9724	003.1331	001.4699
38	$+2.4 \cdot 2\pi$	000.3525	257.9724	003.1331	001.4699
39	$+2.6 \cdot 2\pi$	000.3525	257.9724	003.1331	001.4699
40	$+2.8 \cdot 2\pi$	000.3525	257.9724	003.1331	001.4699
41	$+3.0 \cdot 2\pi$	000.3525	257.9724	003.1331	001.4699
42	$+3.2 \cdot 2\pi$	000.3525	257.9724	003.1331	001.4699
43	$+3.4 \cdot 2\pi$	000.3525	257.9724	003.1331	001.4699
44	$+3.6 \cdot 2\pi$	000.3525	257.9724	003.1331	001.4699
45	$+3.8 \cdot 2\pi$	000.3525	257.9724	003.1331	001.4699
46	$+4.0 \cdot 2\pi$	000.3525	257.9724	003.1331	001.4699
47	$+4.2 \cdot 2\pi$	000.3525	257.9724	003.1331	001.4699
48	$+4.4 \cdot 2\pi$	000.3525	257.9724	003.1331	001.4699
49	$+4.6 \cdot 2\pi$	000.3525	257.9724	003.1331	001.4699
50	$+4.8 \cdot 2\pi$	001.0021	258.0043	002.7945	001.1608
51	$+5.0 \cdot 2\pi$	005.9571	258.0176	002.3280	001.4338

Table 4.5: Equilibrium points $u_{c,i}$ and corresponding prefilter gain values $\mathbf{V}$.

i	$u_{c,i}$	$V_{1,i}$	$V_{2,i}$	$V_{3,i}$	$V_{4,i}$
1	$-5.0 \cdot 2\pi$	041.1791	001.3539	−01.3539	001.3539
2	$-4.8 \cdot 2\pi$	040.1943	001.3784	−01.3784	001.3784
3	$-4.6 \cdot 2\pi$	039.3253	001.4094	−01.4094	001.4094
4	$-4.4 \cdot 2\pi$	038.4925	001.4446	−01.4446	001.4446
5	$-4.2 \cdot 2\pi$	037.7010	001.4849	−01.4849	001.4849
6	$-4.0 \cdot 2\pi$	036.9571	001.5314	−01.5314	001.5314
7	$-3.8 \cdot 2\pi$	036.2687	001.5854	−01.5854	001.5854
8	$-3.6 \cdot 2\pi$	035.6450	001.6487	−01.6487	001.6487
9	$-3.4 \cdot 2\pi$	035.0976	001.7236	−01.7236	001.7236
10	$-3.2 \cdot 2\pi$	035.2888	001.8470	−01.8470	001.8470
11	$-3.0 \cdot 2\pi$	034.2946	001.9213	−01.9213	001.9213
12	$-2.8 \cdot 2\pi$	034.0813	002.0540	−02.0540	002.0540
13	$-2.6 \cdot 2\pi$	034.0325	002.2191	−02.2191	002.2191
14	$-2.4 \cdot 2\pi$	034.1900	002.4283	−02.4283	002.4283
15	$-2.2 \cdot 2\pi$	034.6103	002.6991	−02.6991	002.6991
16	$-2.0 \cdot 2\pi$	035.3720	003.0582	−03.0582	003.0582
17	$-1.8 \cdot 2\pi$	036.5875	003.5488	−03.5488	003.5488
18	$-1.6 \cdot 2\pi$	038.4215	004.2440	−04.2440	004.2440
19	$-1.4 \cdot 2\pi$	041.1227	005.2745	−05.2745	005.2745
20	$-1.2 \cdot 2\pi$	045.0756	006.8925	−06.8925	006.8925
21	$-1.0 \cdot 2\pi$	050.8715	009.6289	−09.6289	009.6289
22	$-0.8 \cdot 2\pi$	059.3081	014.7293	−14.7293	014.7293
23	$-0.6 \cdot 2\pi$	070.4644	025.4392	−25.4392	025.4392
24	$-0.4 \cdot 2\pi$	075.2802	049.7466	−49.7466	049.7466
25	$-0.2 \cdot 2\pi$	021.5949	084.1456	−84.1456	084.1456
26	$\pm 0.0 \cdot 2\pi$	−65.3795	192.2404	−62.5989	−64.2621

Table 4.6: Equilibrium points $u_{c,i}$ and corresponding prefilter gain values $\mathbf{V}$.

i	$u_{c,i}$	$V_{1,i}$	$V_{2,i}$	$V_{3,i}$	$V_{4,i}$
27	$+0.2 \cdot 2\pi$	-71.6925	031.7696	-31.7696	031.7696
28	$+0.4 \cdot 2\pi$	-59.8526	017.0361	-17.0361	017.0361
29	$+0.6 \cdot 2\pi$	-49.7957	010.4396	-10.4396	010.4396
30	$+0.8 \cdot 2\pi$	-42.8320	007.1072	-07.1072	007.1072
31	$+1.0 \cdot 2\pi$	-38.1048	005.2319	-05.2319	005.2319
32	$+1.2 \cdot 2\pi$	-34.8829	004.0847	-04.0847	004.0847
33	$+1.4 \cdot 2\pi$	-32.6877	003.3367	-03.3367	003.3367
34	$+1.6 \cdot 2\pi$	-31.2135	002.8240	-02.8240	002.8240
35	$+1.8 \cdot 2\pi$	-30.2610	002.4583	-02.4583	002.4583
36	$+2.0 \cdot 2\pi$	-29.6965	002.1890	-02.1890	002.1890
37	$+2.2 \cdot 2\pi$	-29.4275	001.9853	-01.9853	001.9853
38	$+2.4 \cdot 2\pi$	-29.3883	001.8277	-01.8277	001.8277
39	$+2.6 \cdot 2\pi$	-29.5312	001.7034	-01.7034	001.7034
40	$+2.8 \cdot 2\pi$	-29.8207	001.6039	-01.6039	001.6039
41	$+3.0 \cdot 2\pi$	-30.2298	001.5229	-01.5229	001.5229
42	$+3.2 \cdot 2\pi$	-30.7378	001.4563	-01.4563	001.4563
43	$+3.4 \cdot 2\pi$	-31.3285	001.4009	-01.4009	001.4009
44	$+3.6 \cdot 2\pi$	-31.9889	001.3543	-01.3543	001.3543
45	$+3.8 \cdot 2\pi$	-32.7086	001.3149	-01.3149	001.3149
46	$+4.0 \cdot 2\pi$	-33.4794	001.2811	-01.2811	001.2811
47	$+4.2 \cdot 2\pi$	-34.2942	001.2521	-01.2521	001.2521
48	$+4.4 \cdot 2\pi$	-35.1474	001.2270	-01.2270	001.2270
49	$+4.6 \cdot 2\pi$	-36.0341	001.2050	-01.2050	001.2050
50	$+4.8 \cdot 2\pi$	-36.3048	001.1651	-01.1651	001.1651
51	$+5.0 \cdot 2\pi$	-32.3294	000.9973	-00.9973	000.9973

Chapter 5

Simulation and Results

5.1 Summary

5.1.1 Summary Table

There are three main events used in this thesis in order to compare the different control structures used in these PLLs.

The first simulated event is a 0.5 [s] long Phase-to-Phase short circuit. For this event, three different scenarios are considered; a Clean (Clean) scenario, with no harmonics nor measurement disturbance; a Low Harmonics (LH) scenario with measurement disturbance; a High Harmonics (HH) scenario with measurement disturbance. While the shortcirucuit is 0.5 [s], the full simulation runs for 1 [s].

The second simulated event is a 30 [s] long Frequency Variation (FreqVar) simulation. The same three different scenarios considered for the Short circuit event are considered for the Frequency Variation event (Clean, LH and HH).

This data is summarised in table 5.1, where certain additional details about the different simulations performed are included.

Table 5.1: Summary table with details about every simulation run.

Event	Short circuit			Freq. Variation		
Scenario	Clean	LH	HH	Clean	LH	HH
Duration (s)	1	1	1	30	30	30
Disturbance	Yes	Yes	Yes	Yes	Yes	Yes
5th Harmonic [%]	00.0	03.0	30.0	00.0	03.0	30.0
7th Harmonic [%]	00.0	01.5	15.0	00.0	01.5	15.0
V_q^+ SS Error $[p.u.]$	$7.4 \cdot 10^{-4}$	$7.4 \cdot 10^{-4}$	$7.4 \cdot 10^{-4}$	$4 \cdot 10^{-2}$	$4 \cdot 10^{-2}$	$4 \cdot 10^{-2}$
Settling Time $[s]$	0.038	0.038	0.038	-	-	-

5.1.2 Effects of Disturbance

Disturbance is included as random noise in the measuring. Figure 5.1 shows the three-phase voltage for the Clean case, with no harmonics or measuring disturbances. The effects of the disturbance in the source voltage can be seen in figure 5.2.

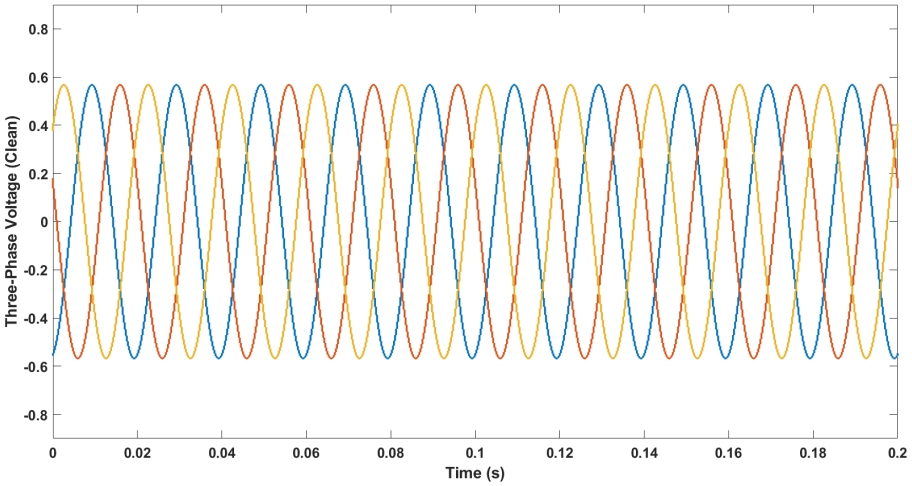

Figure 5.1: Three-phase voltage at the source without measurement disturbance.

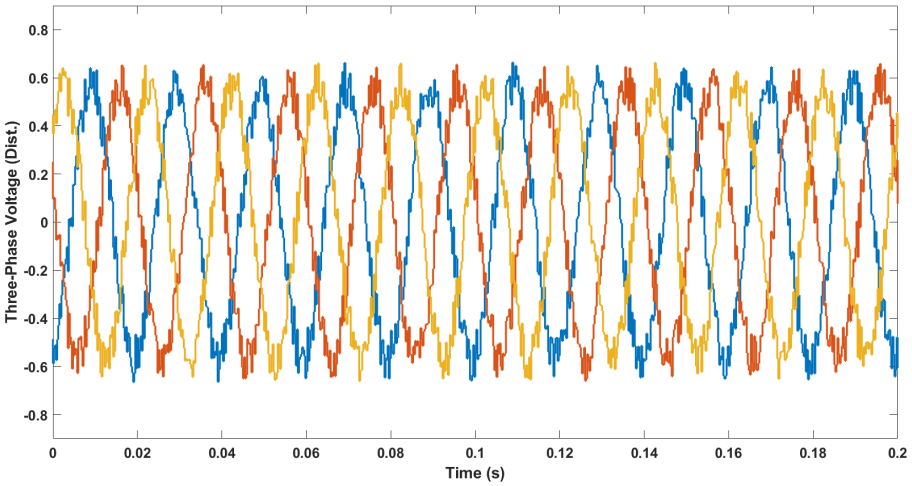

Figure 5.2: Three-phase voltage at the source with measurement disturbance.

Figures 5.2 and 5.3 show that the effects of the disturbance do not affect the PLL's capability of tracking the system's phase.

Due to this, no separate scenarios are dedicated to the disturbance. While its impact is imperceptible, disturbance is included in the Low Harmonics and High Harmonics scenarios.

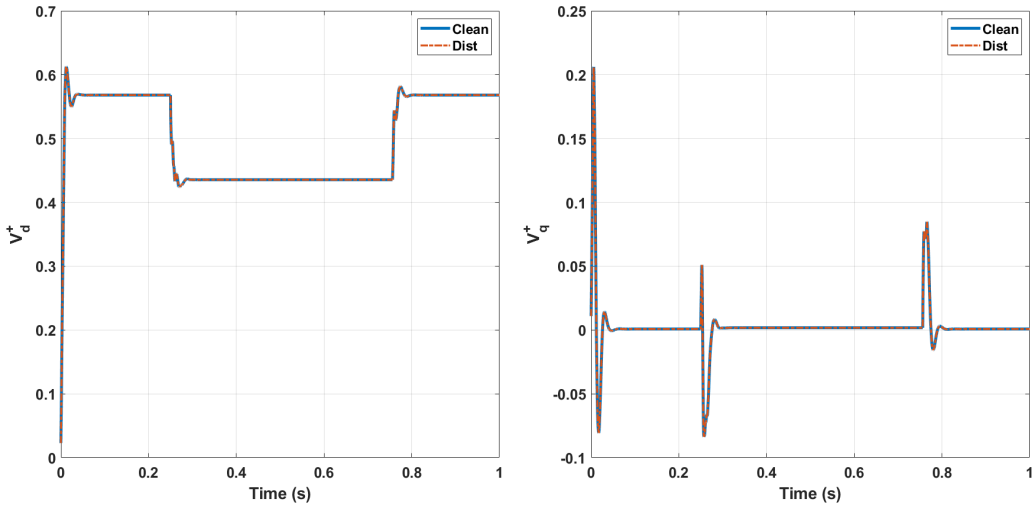

Figure 5.3: Reconstructed voltages $\hat{V}_d^+$ and $\hat{V}_q^+$ with and without measuring disturbance.

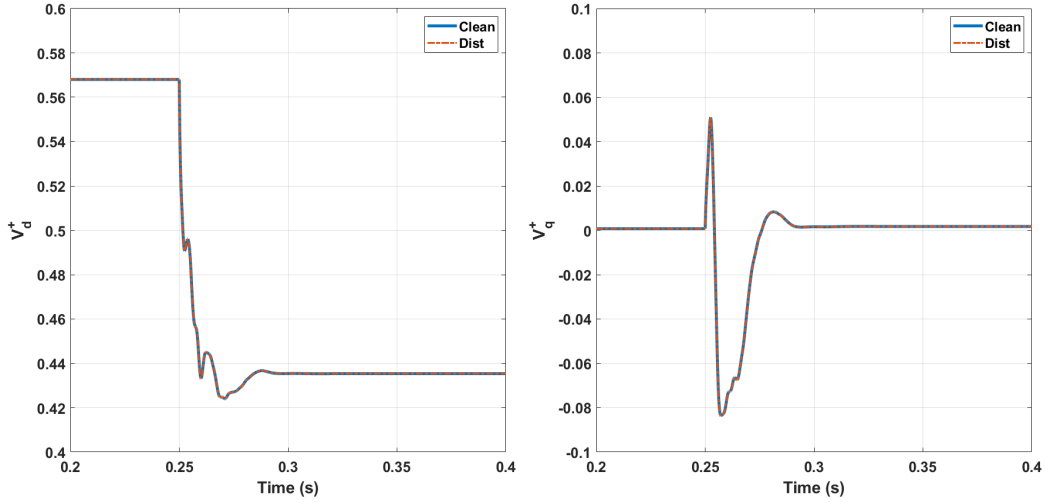

Figure 5.4: Detail of figure 5.2

5.1.3 Effects of Harmonics

Fifth and Seventh harmonics are included in the simulation. Both scenarios include disturbance effects, which is why the exact shape of the base sine wave plus the harmonics is not completely obvious to the eye in the following graphics.

The Low Harmonics scenario includes the fifth harmonic at 3% of the rated voltage value and the seventh harmonic at 1.5% of the rated voltage value. The three phase voltage at the source for the Low Harmonics scenario can be seen in figure 5.5.

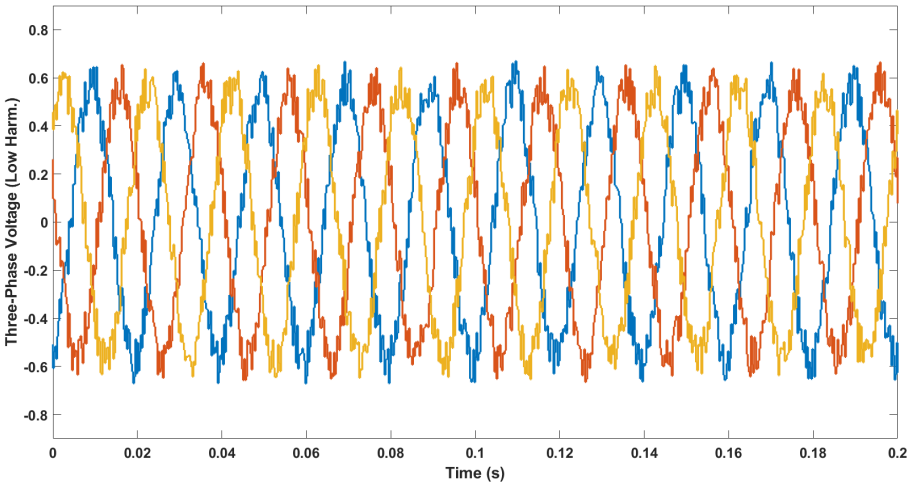

Figure 5.5: Three-phase voltage at the source for the Low Harmonics scenario.

The High Harmonics scenario includes the fifth harmonic at 30% of the rated voltage value and the seventh harmonic at 15% of the rated voltage value. The three phase voltage at the source for the High Harmonics scenario can be seen in figure 5.6.

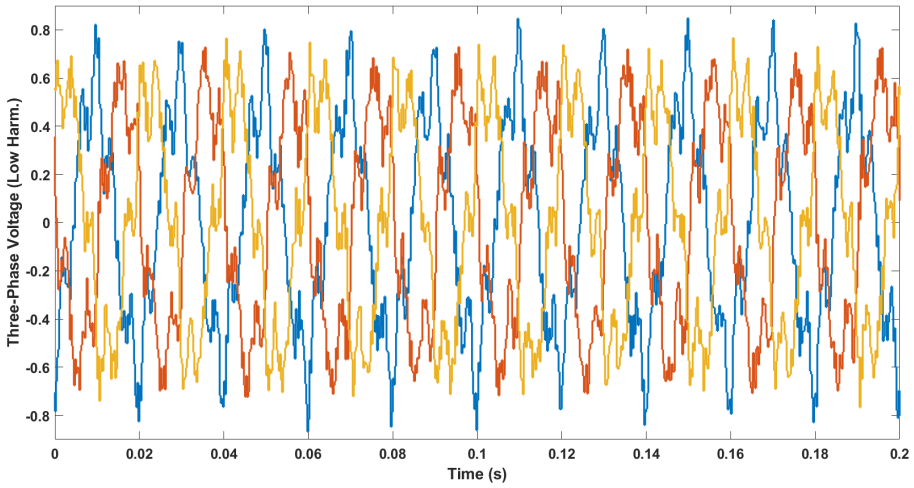

Figure 5.6: Three-phase voltage at the source for the High Harmonics scenario.

5.2 Short Circuit Simulation

5.2.1 Voltage

Figures 5.7, 5.8 and 5.11 show the evolution of V_d^+, V_q^+ and Δf respectively during the full Short Circuit simulation run for the High Harmonics scenario.

A V_d^+ voltage dip of *some p.u.* (*some*% of the steady state value) can be appreciated in figure 5.7 as a result of the Phase-to-Phase short circuit.

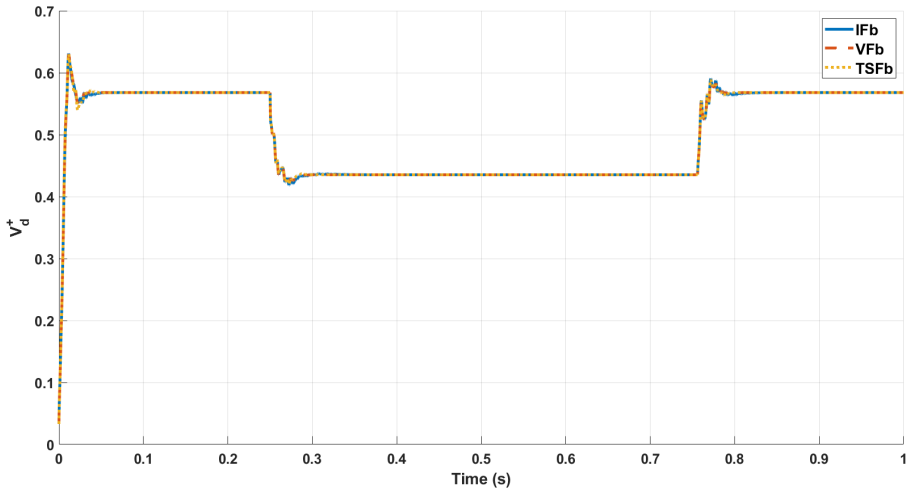

Figure 5.7: V_d^+ voltage for the short circuit High Harmonics scenario.

The I-augmented PLL (IFB) needs a longer time to be able to reach $V_q^+ = 0$ after the short circuit event, although it is the only one that does it without steady state error. The Static

Prefilter (VFb) and the Takagi-Sugeno Static Prefilter (TSFb) show steady state errors of *value* and *value p.u.* respectively. This can be appreciated in figure 5.8 below.

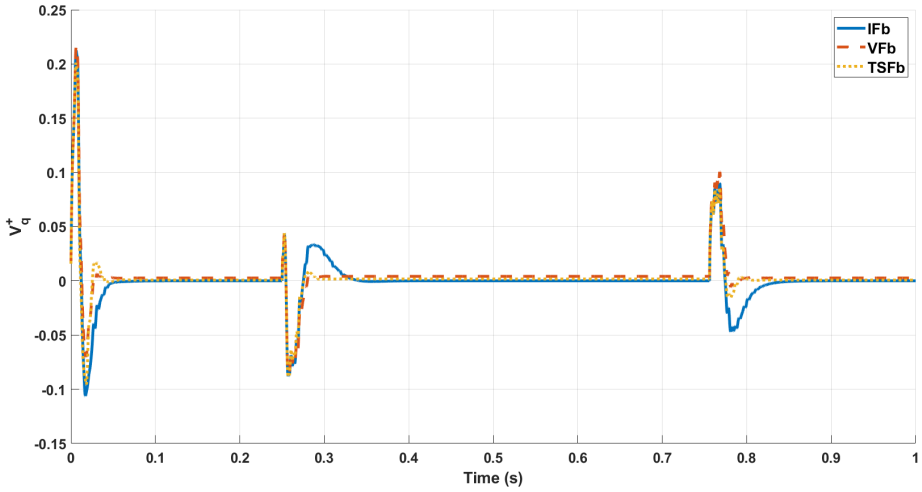

Figure 5.8: V_q^+ voltage for the short circuit High Harmonics scenario.

In order to show the transition that the systems undergo during the short-circuit event, figures 5.9 and 5.10 show the transition period in detail.

The I-augmented PLL's (IFb) longer settling time can be better seen in figure 5.9.

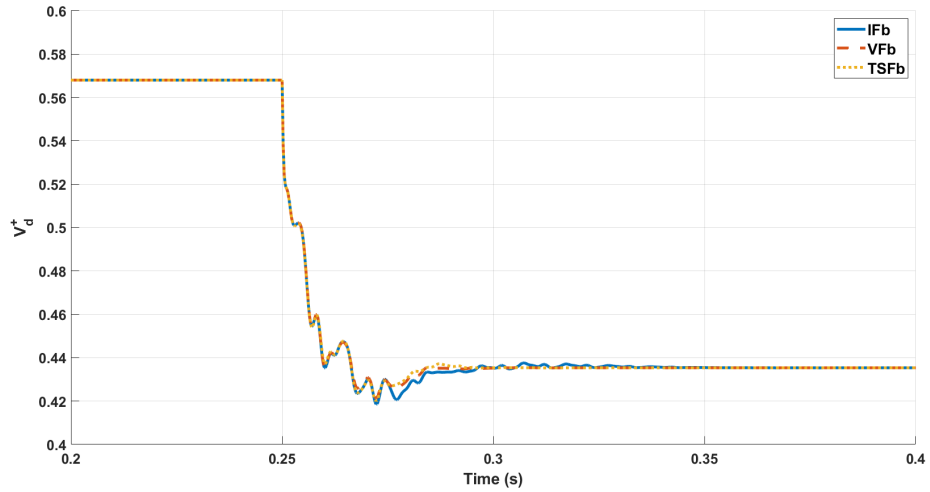

Figure 5.9: Detail of the V_d^+ voltage for the short circuit High Harmonics scenario.

The I-augmented PLL's (IFb) overshoot and longer settling times in V_q^+ can be appreciated in figure 5.10 together with the Static Prefilter (VFb) and Takagi-Sugeno Prefilter (TSFb) steady-state error.

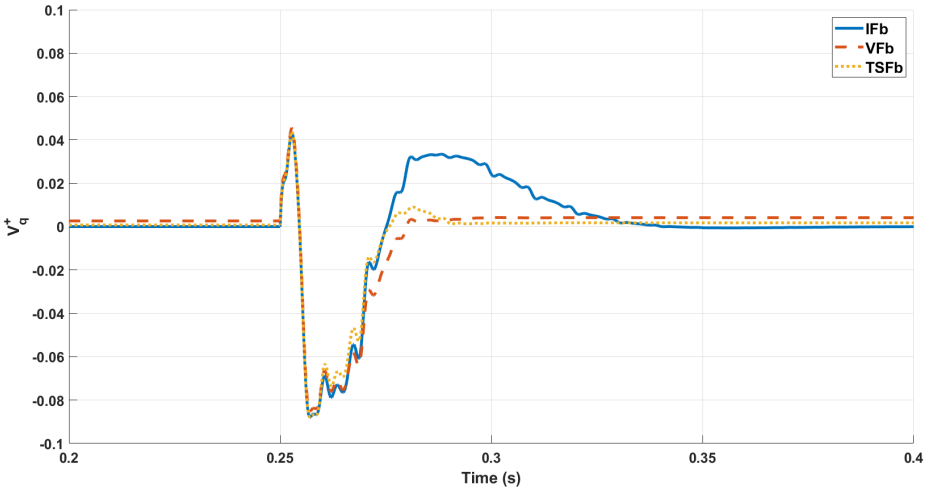

Figure 5.10: Detail of the V_q^+ voltage for the short circuit High Harmonics scenario.

The graphs for the Low Harmonics and Clean scenarios have not been included since the results are very similar. Some of these figures have been included in section 5.4 at the end of this chapter in order to show how similar the results are for the different scenarios.

5.2.2 Frequency

All three PLL systems are able to reach the target steady state frequency of 50 $[Hz]$, as seen in figure 5.11.

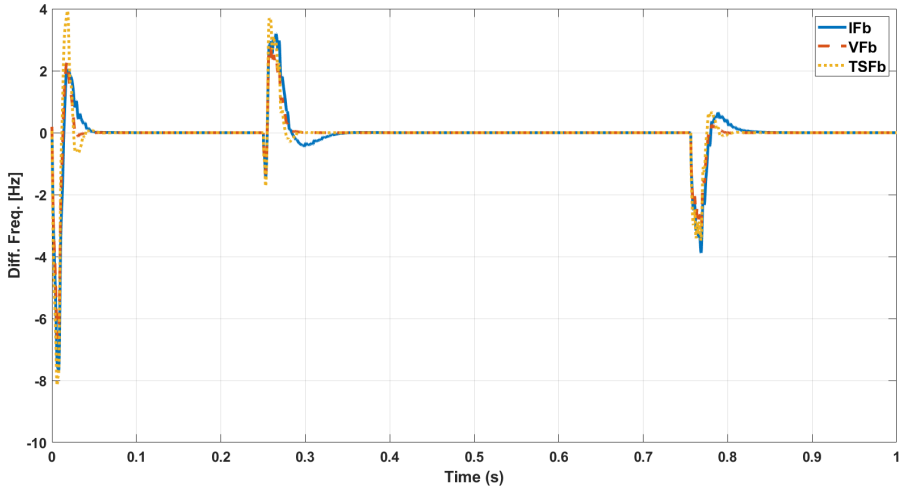

Figure 5.11: Δf for the short circuit High Harmonics scenario.

5.2.3 Settling Times

In this section the results regarding the initial transient are shown.

The settling time needed by each of the PLLs in order to reach the target steady state value seen in table 5.1 is graphically represented in figures 5.12 and 5.13 below.

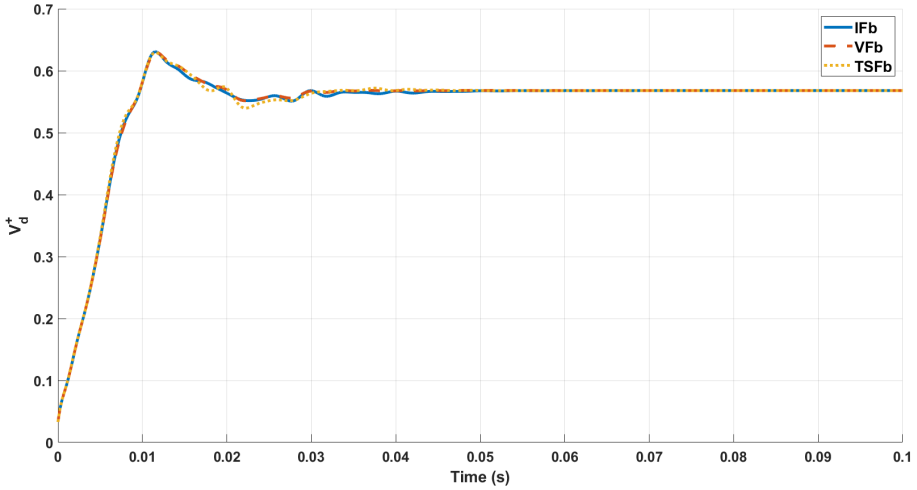

Figure 5.12: V_d^+ voltage in the initial transient for the short circuit High Harmonics scenario.

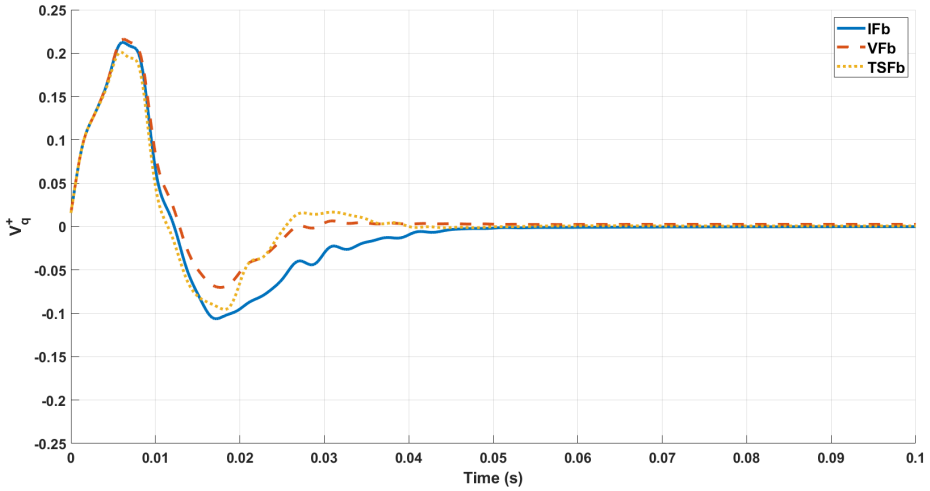

Figure 5.13: V_q^+ voltage in the initial transient for the short circuit High Harmonics scenario.

5.3 Frequency Variation Simulation

5.3.1 Frequency

The evolution of the source frequency during the full Frequency Variation simulation run can be seen in figure 5.14 below.

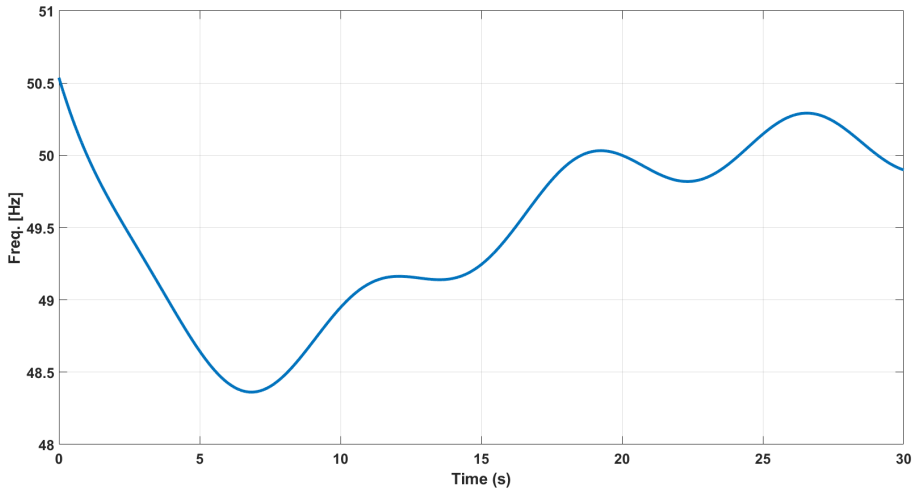

Figure 5.14: Evolution of the original source frequency during the Frequency Variation event.

All three PLL systems are able to reach different target steady state frequencies. Still, the Static Prefilter (VFb) and Takagi Sugeno (TSFb) PLLs show small steady state errors that range from 2 to -6 mHz, as seen in figure 5.15.

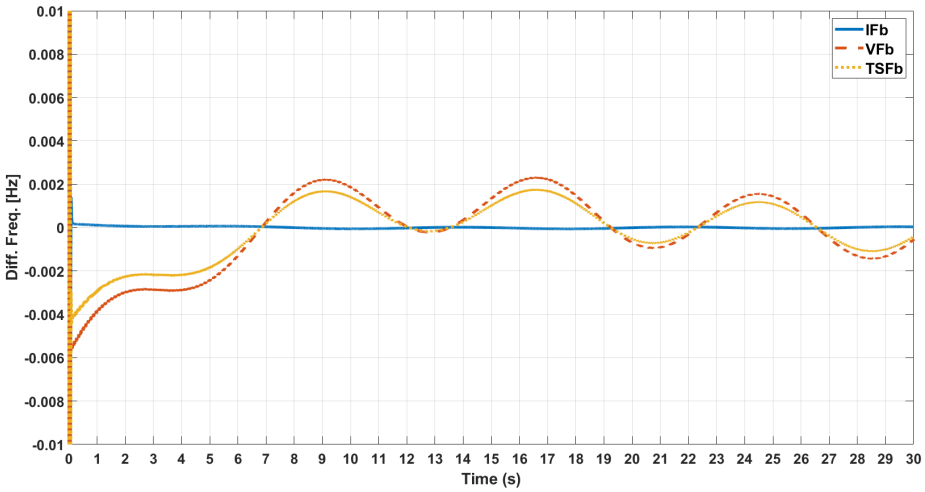

Figure 5.15: Δf for the frequency variation High Harmonics scenario.

5.3.2 Voltage

Figures 5.16 and 5.17 show the evolution of V_d^+ and V_q^+ respectively during the full Frequency Variation simulation run for the High Harmonics scenario.

A difference between the V_d^+ voltages between the three PLLs can be appreciated in figure 5.16.

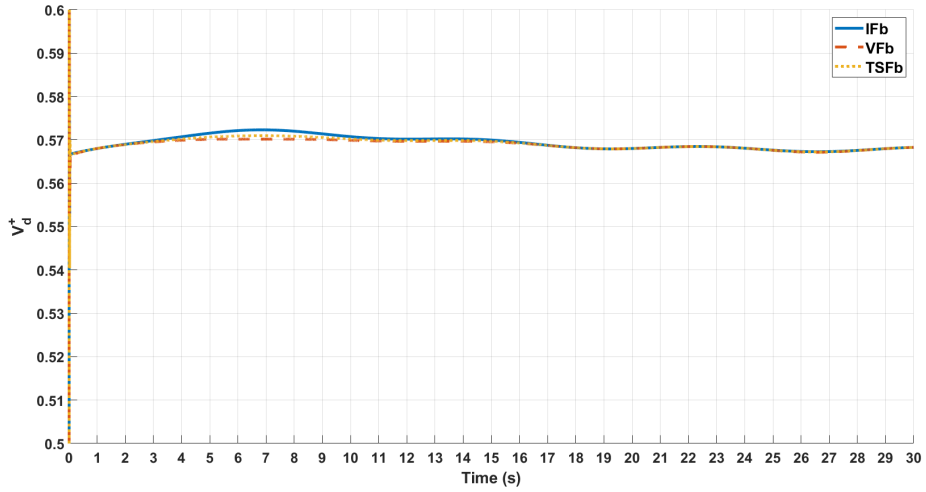

Figure 5.16: V_d^+ voltage for the frequency variation High Harmonics scenario.

The Static Prefilter (VFb) and the Takagi-Sugeno (TSFb) PLLs are not able to obtain $V_q^+ = 0$ when the frequency deviates from 50 $[Hz]$. This steady state error can be seen in figure 5.17.

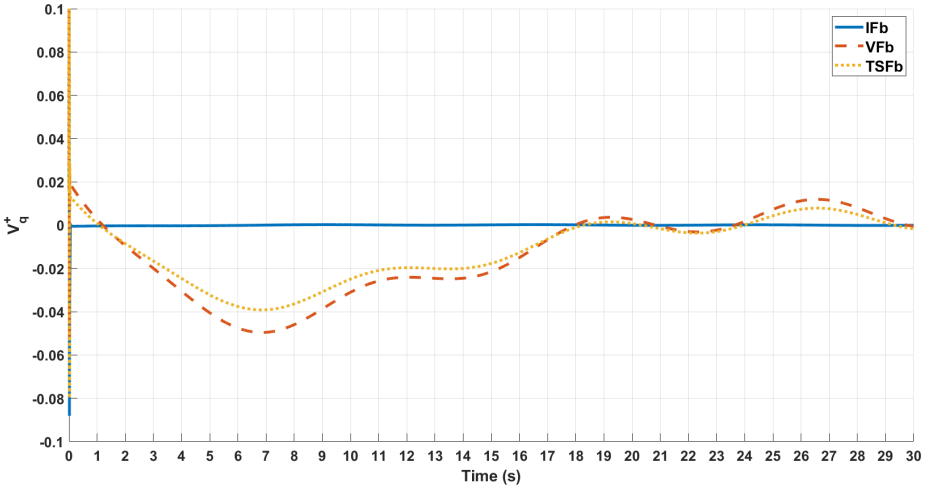

Figure 5.17: V_q^+ voltage for the frequency variation High Harmonics scenario.

The graphs for the Low Harmonics and Clean scenarios have not been included since the results are very similar. Some of these figures have been included in section 5.4 at the end of this chapter in order to show how similar the results are for the different scenarios.

5.4 Clean and Low Harmonics results

These results are very similar to those of the frequency variation event for the high harmonics scenario. Results for the high harmonics scenario are the only shown in detail in the Results chapter.

In this section only the simulation results pertaining to the frequency variation event for the clean and low harmonics scenarios are shown. It is deemed unnecessary to include shortcircuit results because the purpose of this section is to show the high similarity between the clean and low harmonics scenarios, to justify the fact that they were not included in more detail.

The evolution of V_d^+ and V_q^+ for the clean and low harmonics scenarios are shown in figures 5.18 and 5.19 respectively.

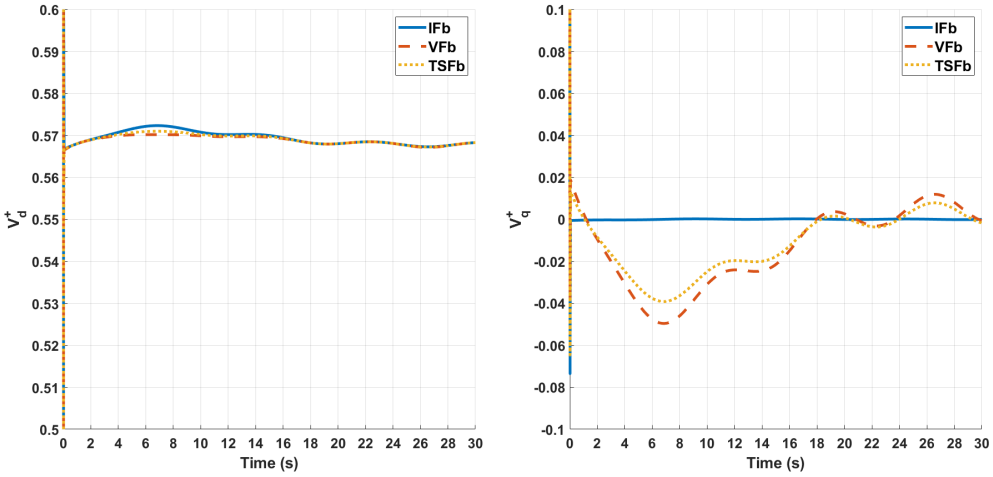

Figure 5.18: V_d^+ and V_q^+ voltages for the frequency variation Clean scenario.

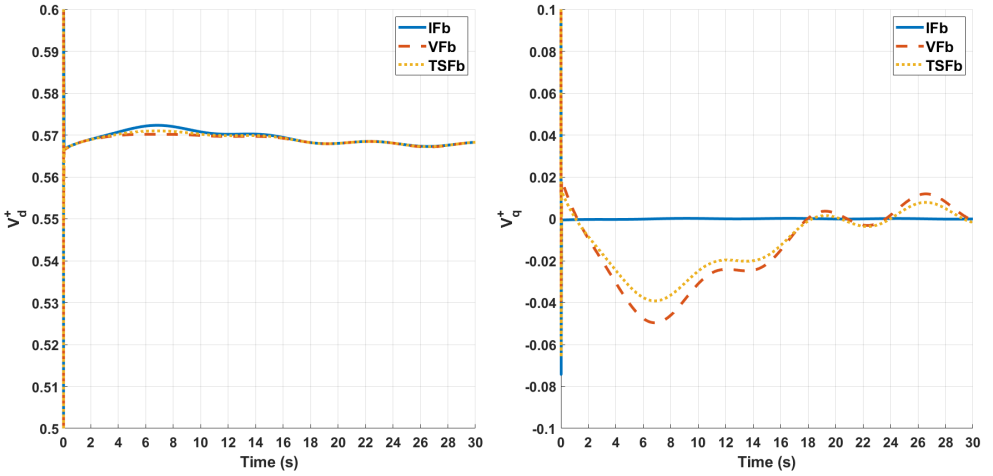

Figure 5.19: V_d^+ and V_q^+ voltages for the frequency variation Low Harmonics scenario.

The evolution of the frequency difference Δf of both cases is shown in figure 5.20.

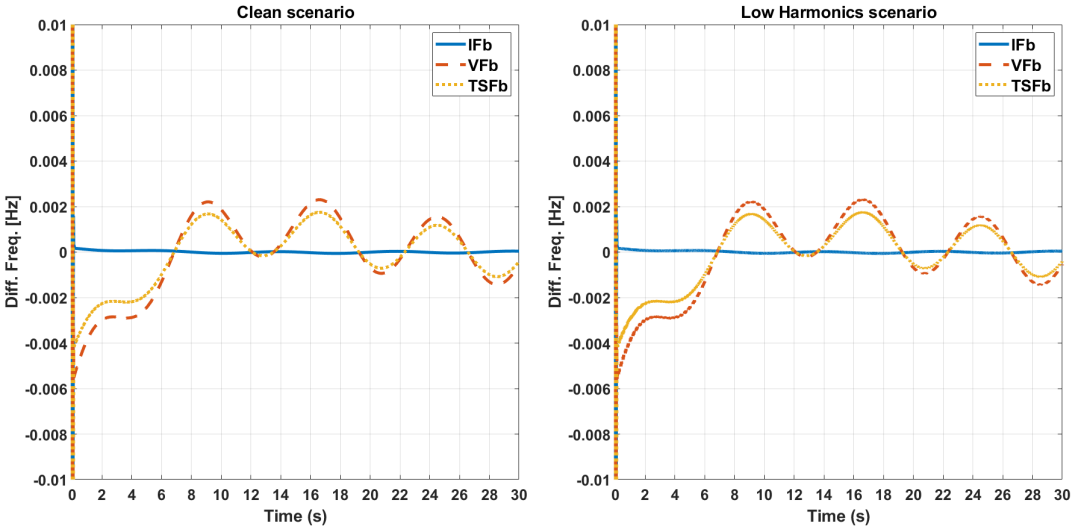

Figure 5.20: Evolution of Δf for the frequency variation even for the Clean and Low Harmonics scenarios.

Chapter 6

Conclusions and Discussion

6.1 Conclusions

During the course of this Master's thesis done during a research assistance internship at HTW Berlin, a Takagi-Sugeno Static Prefilter LMS PLL has been developed and implemented in MatLab® 2019a Simulink

Using an electrical modelling environment and the I-Augmented and Standard Prefilter PLL environments already developed by HTW Berlin's Nico Goldschmidt during the course of his PhD work, shortcircuit, load jump and frequency variation events have been simulated under different disturbance and harmonics scenarios. Shortcircuit and Frequency Variation simulation results have been included in this Master's thesis in order to show the capabilities of the TS Static Prefilter for phase tracking purposes.

The Least Mean Squares filter used for the reconstruction of the main harmonic, while necessary and important for the results obtained by the different PLLs studied in this thesis, is not part of the scope of this thesis since it was not developed during the course of it, but done before by the system control research group at HTW Berlin.

6.2 Discussion

6.2.1 Comparison of Takagi-Sugeno Static Prefilter and I-Augmented

For the shortcircuit event, the Takagi-Sugeno Static Prefilter PLL requires 0.038 $[s]$ in order to reach the steady state value, while the I-Augmented PLL requires 0.082 $[s]$. Overshoot during the shortcircuit event is also smaller for the TS Static Prefilter, being of 0.009 $p.u.$ while the I-Augmented presents an overshoot of 0.031 $p.u.$. This can be seen in figure 5.10 in section 5.2.1.

While the TS Static Prefilter PLL is faster that the I-Augmented PLL, during the shortcircuit event simulations the TS Static Prefilter shows a permanent steady state error at the V_q^+ voltage of $7.4 \cdot 10^{-4}$ $p.u.$.

This error increases during the frequency variation event, where it can be seen that when the difference between the source frequency and the reference frequency (50 Hz) increases, so does

the V_q^+ steady state error. The biggest steady state error for the TS Static Prefilter happens at 7 s, reaching -0.04 $p.u.$. This can be seen in figure 5.15 in section 5.3.1.

6.2.2 Comparison of Takagi-Sugeno Static Prefilter and Standard Static Prefilter

For the shortcircuit event, the Takagi-Sugeno Static Prefilter PLL requires 0.038 [s] in order to reach the steady state value, while the Standard Static Prefilter requires 0.051 [s]. Overshoot during the shortcircuit event is bigger for the TS Static Prefilter, being of 0.009 $p.u.$ while the Standard Static Prefilter presents no overshoot. This can be seen in figure 5.10 in section 5.2.1.

The TS Static Prefilter PLL is not only faster that the Standard Static Prefilter, but it's steady state error is also smaller. While the TS Static Prefilter PLL shows V_q^+ voltage steady state error of $7.4 \cdot 10^{-4}$ $p.u.$, the Standard Static Prefilter PLL's error is of $2.6 \cdot 10^{-3}$ $p.u.$.

This error increases during the frequency variation event, where it can be seen that when the difference between the source frequency and the reference frequency (50 Hz) increases, so does the V_q^+ steady state error. The biggest steady state error happens at 7 s, reaching -0.04 $p.u.$ for the TS Static Prefilter and -0.05 $p.u.$ for the Standard Static Prefilter. This can be seen in figure 5.15 in section 5.3.1.

6.2.3 Improvements for the Takagi-Sugeno Static Prefilter

The simulation results obtained show that using a Takagi-Sugeno Static Prefilter PLL offers several advantages compared to the two other PLLs used, like faster response time than the I-augmented PLL and smaller Steady State error than the Standard Static Prefilter PLL. Even though the Takagi-Sugeno PLL still shows some Steady State error and overshoot in response to faults, there is room for improvement.

While design parameters for pole placement α, β and θ have been optimized up to a certain point, they have not been optimized for each of the linearised models used for the Takagi-Sugeno Static Prefilter PLL.

Including more linearised models in the Takagi-Sugeno Static Prefilter PLL could help reduce the steady state error, but during the development of this thesis the use of more linearised models (between 50 and 200) has not shown better results.

The combination of more linearised models and individualised pole placement design parameters might improve the results of the Takagi-Sugeno Static Prefilter PLL.

Acknowledgements

En primer lugar me gustaría agradecer a Oriol Gomis de CITCEA-UPC y a Horst Schulte del grupo de investigación de control de HTW-Berlin por darme la oportunidad de llevar a cabo este trabajo de fin de máster. También es imprescindible agradecer la ayuda prestada en todo momento por Nico Goldschmidt de HTW-Berlin, cuyos consejos, experiencia y apoyo han sido claves para poder llevar acabar este trabajo. Agradezco también además de a Horst y a Nico al resto del grupo de control de HTW-Berlin el haberme recibido en Berlín estos meses a pesar de las circunstancias adversas debido a la pandemia.

En segundo lugar, quiero agradecer el ininterrumpido apoyo recibido por mi pareja Hanneke y mi familia, con un agradecimiento especial a mis hermanos Agustín, Tomás y Lourdes, mis padres Ángeles y Andrés, mi abuela Alicia, mi tía Isabel y mi abuelo Francisco Javier (q.e.p.d.), sin cuyo cariño en la distancia no hubiese sido posible llegar a dónde estoy hoy.

Por último, me gustaría agradecer la compañía de toda la gente que hace que el estudio y el trabajo sean más llevaderos. Amigos de Mallorca, compañeros de clase, proyectos y estudio, compañeros de piso y sin falta a las antracitas, hullas y demás carbones de la panda; todos compañeros de una etapa de mi vida que recordaré con gusto.

Appendix A

Appendix

A Environmental impact

A.1 Isolated grids and sustainability

Isolated electrical power systems present a series of characteristics that distinguish their environmental impact from standard grids.

This section focuses on both how isolated power systems behave regarding CO_2 emissions (direct impact) and how complications arise when trying to tackle such an issue via the implementation of renewable energy sources.

Isolated electrical grids are usually located at remote or uncommunicated locations because of bodies of water, mountains or political situations. Such systems, are characterized by a low inertia due to a decreased number of generators and interconnections. This means that traditional thermal generation systems provide not only energy but stability. Fossil fuel consumption contributes to global warming and climate change, and the use of traditional generation in these systems is the standard.

In the case of insular electrical power systems, the environmental effects are aggravated by a series of factors tied to their isolation and economy.

To the emissions caused by fossil fuel burning it is important to also add those caused by the transport of the different fuels to the island. Fossil fuel generation usually represents most if not all of the generation of an island, so this is not a negligible source of CO_2.

Grid quality should also be factored in when talking about the CO_2 emissions of insular systems. Generating facilities in insular systems are generally old and relatively outdated when compared to more modern, efficient facilities.

Transmission losses are also another point to focus on when talking about the lack of efficiency of insular grids. A lot of isolated systems (particularly islands) tend to rely heavily on tourism; this means that placing power plants close to where power is consumed is not an option, so transmission losses are higher than usual. The Majorcan grid is a clear example of this, with one of its stations with the highest rated power (Es Murterar, 530MW [21]) is placed in a relatively far and isolated bus of the grid.

The dependency on fossil fuel imports and its effects on the environment call for a solution that is extremely common nowadays; the implementation of clean, renewable energy sources in the power system. This would be a possible solution for insular grids if not for their security and stability issues; voltage and frequency deviations are quite problematic due to the insular systems' characteristically low inertia.

Renewable energy sources like photo-voltaic and wind generation both generate no carbon emissions once they are functioning, but they are also unreliable and intermittent. This means that they cannot provide the inertia these fragile grids need; in fact, they may even worsen the situation of these issues.

A.2 The importance of control systems

The characteristics of microgrids and isolated grids with high penetration of intermittent renewable energy sources like wind or photo-voltaic make them unstable and unreliable in comparison to mainland grids [8].

This means that the introduction of robust control systems is necessary. Being able to provide reliability to the grid even under uncertain circumstances means that the dependency on traditional generation systems decreases. As such, the use of fossil fuels and the emissions tied to their transport and consumption can be reduced.

B Budget

B.1 Labour costs

Labour costs are divided depending on the type of work performed. Costs vary among them depending on the type of work and the specialization and information needed to perform such task.

The details are as follows:

1. *Research.* This includes the hours dedicated to the gathering of information concerning the state of the art, the situation of insular grids and details on various of the models included. A cost of 12 €/ho has been considered because some previous knowledge is needed in order to know what type of documentation to look for and the interpretation needed after reading.
2. *Modelling.* This includes the hours dedicated to the mathematical modelling and the implementation of the models in the different software used during the development of this thesis. A cost of 24 €/h has been considered because of the technical and theoretical knowledge needed to design and implement the various models.
3. *Simulation.* This includes the hours dedicated to running the simulations and making sure that they function as they should during the development of this thesis. A cost of 6 €/h has been considered because during the time that simulations are running it is possible to multitask, allowing for *Research* and *Writing* to be done while the software runs the various simulations on the background.

4. *Analysis.* This includes the hours dedicated to interpreting the results of the simulations and its consequences in regards to the topic studied during the development of this thesis. A cost of 28 €/h has been considered because it is the key aspect of the thesis and it is heavily dependant on the work done previously during the *Research* and *Modelling* phases.

5. *Writing.* This includes the hours dedicated to learning LaTeX, writing and revising this thesis. A cost of 9 €/h because this phase is not as technical as others.

Table A.1: Labour costs

Concept	**Hourly rate[€/h]**	**Units** (h)	**Cost**(€)
Research	12	250	3,000
Modelling	24	240	5,760
Simulation	6	140	840
Analysis	28	80	2,240
Writing	9	130	1170
Subtotal		840	13,010
VAT(21%)			2,732
Total			15,742

B.2 Developement tools and office material

The cost of the equipment and software used during the development of this thesis is included here. The cost of IEEE articles or other literature material is not included, as the university provides free access to those contents.

Amortization for each item is calculated as follows:

1. *Personal computer.* An eight years long life expectancy is considered and eleven months have been dedicated to the development of this thesis.

2. *Matlab®license.* A year-long license is considered, and seven months have been dedicated to the development of this thesis.

B.3 Total cost

Considering the labour costs listed in table A.1 and the development tools and equipment listed in table A.2, the total cost is as seen in table A.3.

Table A.2: Development costs

Concept	**Unit cost[€/ut]**	**Units**	**Cost(€)**	**Amortization (€)**
Personal computer	439.90	1	779.90	89.36
MatLab® 2015b (Academic use)	500	1	500	291.66
Subtotal				381
VAT(21%)				80
Total				461

Table A.3: Total cost

Item	**Cost[€]**
Labour	15,742
Development tools and equipment	461
Total (VAT included)	**16,203**

Bibliography

[1] Mahmoud Chilali and Pascal Gahinet. H design with pole placement constraints: an lmi approach. *Automatic Control, IEEE Transactions on*, 41:358 – 367, 03 1996. ix, 9, 10

[2] Nico Goldschmidt and Horst Schulte. Estimation of grid frequency in disturbed converter-based power systems by pll state variable feedback. In *Estimation of Grid Frequency in Disturbed Converter-Based Power Systems by PLL State Variable Feedback*, 07 2020. ix, 1, 2, 9, 11, 13, 29

[3] Eduard Bullich-Massagué, Francisco-Javier Cifuentes-García, Ignacio Glenny-Crende, Marc Cheah-Mañé, Mònica Aragüés-Peñalba, Francisco Díaz-González, and Oriol Gomis-Bellmunt. A review of energy storage technologies for large scale photovoltaic power plants. *Applied Energy*, 274:115213, 2020. 1

[4] H. M. M. Alhaj, N. M. Nor, V. S. Asirvadam, and M. F. Abdullah. Power system harmonics estimation using lms, lmf and lms/lmf. In *2014 5th International Conference on Intelligent and Advanced Systems (ICIAS)*, pages 1–5, 2014. 1

[5] Norbert Klaes, Nico Goldschmidt, and Jens Fortmann. Voltage fed control of distributed power generation inverters with inherent service to grid stability. *Energies*, 13(10), 2020. 1

[6] F. Zhong and Y. Liu. Research on power harmonic reconstruction using compressed sensing. In *2020 39th Chinese Control Conference (CCC)*, pages 2974–2979, 2020. 1

[7] J. Wang, Fan Yang, and Xuhao Du. Microgrid harmonic and interharmonic analysis algorithm based on cubic spline interpolation signal reconstruction. In *IEEE PES Innovative Smart Grid Technologies*, pages 1–5, 2012. 1

[8] Leony Ortiz, Jorge W. González, Luis B. Gutierrez, and Orestes Llanes-Santiago. A review on control and fault-tolerant control systems of ac/dc microgrids. *Heliyon*, 6(8):e04799, 2020. 1, 2, 72

[9] Se-Kyo Chung. A phase tracking system for three phase utility interface inverters. *IEEE Transactions on Power Electronics*, 15(3):431–438, 2000. 2, 9

[10] L. G. Barbosa Rolim, D. Rodrigues da Costa, and M. Aredes. Analysis and software implementation of a robust synchronizing pll circuit based on the pq theory. *IEEE Transactions on Industrial Electronics*, 53(6):1919–1926, 2006. 2

[11] P. Rodriguez, J. Pou, J. Bergas, J. I. Candela, R. P. Burgos, and D. Boroyevich. Decoupled double synchronous reference frame pll for power converters control. *IEEE Transactions on Power Electronics*, 22(2):584–592, 2007. 2

[12] L. Xu, Y. Han, M. M. Khan, Lidan Zhou, Gang Yao, C. Chen, and J. Pan. A novel control strategy for dynamic voltage restorer using decoupled multiple reference frame pll (dmrf-pll). *WSEAS TRANSACTIONS on SYSTEMS archive*, 8:261–277, 2009. 2

[13] X.-G Zhang, D.-K Duan, J.-M Chen, Y.-C Liu, and D.-G Xu. A robust synchronization method for grid sequence extraction. *Przeglad Elektrotechniczny*, 89:101–109, 01 2013. 2

[14] A. K. Pradhan, A. Routray, and A. Basak. Power system frequency estimation using least mean square technique. *IEEE Transactions on Power Delivery*, 20(3):1812–1816, 2005. 2

[15] Otto Föllinger. *Regelungstechnik: Einführung in die Methoden und ihre Anwendung*. VDE VERLAG GMBH, Berlin, 12., überarbeitete auflage edition, 2016. 9, 11, 12, 13, 14, 15, 16

[16] T. Takagi and M. Sugeno. Fuzzy identification of systems and its applications to modeling and control. *IEEE Transactions on Systems, Man, and Cybernetics*, SMC-15(1):116–132, 1985. 17

[17] Zsófia Lendek, Thierry Marie Guerra, Robert Babuška, and Bart de Schutter. Stability Analysis and Nonlinear Observer Design Using Takagi-Sugeno Fuzzy Models. 262, 2011. 17, 19, 20, 21

[18] H. O. Wang, K. Tanaka, and M. F. Griffin. An approach to fuzzy control of nonlinear systems: stability and design issues. *IEEE Transactions on Fuzzy Systems*, 4(1):14–23, 1996. 21

[19] Agustí Egea-Alvarez, Adrià Junyent-Ferré, and Oriol Gomis-Bellmunt. *Active and Reactive Power Control of Grid Connected Distributed Generation Systems*, pages 47–81. Springer Berlin Heidelberg, Berlin, Heidelberg, 2012. 23, 24

[20] P. Kundur. *Power System Stability and Control*. New York : McGraw-Hill, 1994. 23, 24

[21] Red Eléctrica de España. Red de transporte balear. `http://www.ree.es/es/actividades/sistema-electrico-balear/red-de-transporte`. [Online; accessed 12-April-2021]. 71